Astronomy & Astrophysics manuscript no. PMA˙I˙AA˙Submitted
June 26, 2014
© ESO 2014

arXiv:1406.6536v1 [astro-ph.IM] 23 Jun 2014

Polarization measurements analysis

I. Impact of the full covariance matrix on polarization fraction and angle measurements

L. Montier[1,2], S. Plaszczynski[3], F. Levrier[4], M. Tristram[3], D. Alina[1,2], I. Ristorcelli[1,2], J.-P. Bernard[1,2]

[1] Université de Toulouse, UPS-OMP, IRAP, F-31028 Toulouse cedex 4, France
[2] CNRS, IRAP, 9 Av. colonel Roche, BP 44346, F-31028 Toulouse cedex 4, France
[3] Laboratoire de l'Accélérateur Linéaire, Université Paris-Sud 11, CNRS/IN2P3, Orsay, France
[4] LERMA/LRA - ENS Paris et Observatoire de Paris, 24 rue Lhormond, 75231 Paris Cedex 05, France

Preprint online version: June 26, 2014

ABSTRACT

With the forthcoming release of high precision polarization measurements, such as from the *Planck* satellite, the metrology of polarization needs to improve. In particular, it is important to take into account full knowledge of the noise properties when estimating polarization fraction and polarization angle, which suffer from well-known biases. While strong simplifying assumptions have usually been made in polarization analysis, we present a method for including the full covariance matrix of the Stokes parameters in estimates for the distributions of the polarization fraction and angle. We thereby quantify the impact of the noise properties on the biases in the observational quantities. We derive analytical expressions for the probability density functions of these quantities, taking into account the full complexity of the covariance matrix, including the Stokes I intensity components. We perform Monte Carlo simulations to explore the impact of the noise properties on the statistical variance and bias of the polarization fraction and angle. We show that for low variations ($< 10\%$) of the effective ellipticity between the Q and U components around the symmetrical case the covariance matrix may be simplified as is usually done, with negligible impact on the bias. For signal-to-noise ratios on intensity lower than 10 the uncertainty on the total intensity is shown to drastically increase the uncertainty of the polarization fraction but not the relative bias of the polarization fraction, while a 10% correlation between the intensity and the polarized components does not significantly affect the bias of the polarization fraction. We compare estimates of the uncertainties affecting polarization measurements, addressing limitations of estimates of the S/N, and we show how to build conservative confidence intervals for polarization fraction and angle simultaneously. This study, which is the first of a set of papers dedicated to the analysis of polarization measurements, focuses on the basic polarization fraction and angle measurements. It covers the noise regime where the complexity of the covariance matrix may be largely neglected in order to perform further analysis. A companion paper focuses on the best estimators of the polarization fraction and angle, and their associated uncertainties.

Key words. Polarization – Methods: data analysis – Methods: statistical

1. Introduction

Linear polarization measurements are usually decomposed into their Stokes components (I, Q, and U), from which one can derive polarization fraction (p) and angle (ψ). However, these are known to be potentially biased quantities, as first discussed by Serkowski (1958). At its most fundamental level this arises because p is constrained to be positive, while ψ is a non-linear function of the ratio of Q and U, and hence even if Q and U are Gaussian distributed, p and ψ will not be so simple.

While it is advisable to work as much as possible with the Stokes parameters to avoid such issues, it is sometimes more convenient to use the coordinates p and ψ when connecting polarization data to physical models and interpretations. For instance, we may be interested in the maximum fraction of polarization p observed in our Galaxy or the correlation between the polarization fraction and the structure of the magnetic field, which is not easy to carry out over large regions of the sky when using the Stokes parameters. Thus, many authors, e.g., Wardle & Kronberg (1974), Simmons & Stewart (1985) and more recently Vaillancourt (2006) and Quinn (2012), have suggested ways of dealing with polarization fraction estimates to try to correct for the biases. Vinokur (1965) was the first to focus on the polarization angle, with later papers by Clarke et al. (1993) and Naghizadeh-Khouei & Clarke (1993). In all such studies there have been strong assumptions made about the noise properties of the polarization measurements. The noise on the Q and U components are usually considered to be fully symmetric and with no correlation between them, and furthermore the intensity is always assumed to be perfectly known. These assumptions, which we will call the "canonical simplifications," can be useful in practice, in that they allow for rapid progress, but on the other hand they are often simply not correct assumptions to make.

Our work is motivated by the need to understand polarization emission data at microwave to sub-millimetre wavelengths, although the analysis is general enough to be applied to any kind of polarization data. Nevertheless, the details of experimental setup design cannot be ignored, since they affect how correlated are the data. Because the computation of the Stokes parameters and their associated uncertainties strongly depends on the instrumental design, technical efforts have been made to limit the impact of the instrumental systematics. For example, single-dish instruments such as STOKES (Platt et al. 1991), Hertz (Schleuning et al. 1997), SPARO (Renbarger et al. 2004) or SCU-Pol (Greaves et al. 2003) had to face strong systematics due to noise correlation between orthogonal components and atmo-

spheric turbulence, while the SHARP optics (Li et al. 2008) allowed the SHARC-II facility (Dowell et al. 1998) at the Caltech Submillimeter Observatory to be converted into a dual-dish experiment to avoid such noise correlation issues. Nevertheless polarization measurements obtained until now were limited by systematics and statistical uncertainties. Even in some of the most recent studies no correction for the bias of the polarization fraction was applied (e.g., Dotson et al. 2010), or only high signal-to-noise ratio (hereafter S/N) data were used for analysis ($p/\sigma > 3$) in order to avoid the issue (e.g., Vaillancourt & Matthews 2012). One naturally wonders wether this common choice of S/N greater than 3 is relevant for all experiments, and how the noise correlation between orthogonal Stokes components or noise asymmetry between the Stokes parameters could impact this choice.

A major motivation for studying polarized emission in microwaves is the extraction of the weak polarization of the cosmic microwave background. It has been demonstrated by the balloon-borne Archeops (Benoît et al. 2004) experiment and via polarization observations by the *WMAP* satellite (Page et al. 2007) that the polarized cosmological signal is dominated by Galactic foregrounds at large scales and intermediate latitude (with a polarization fraction of 3–10%). Thus the characterization of polarized Galactic dust emission in the submillimetre range has become one of the challenges for the coming decade. This is in order to study the role of magnetic fields for the dynamics of the interstellar medium and star formation, as well as for characterizing the foregrounds for the cosmological polarization signal. The limitations of instrumental specifications and data analysis are therefore being continually challenged. Fully mapping the polarization fraction and angle at large scales is going to be a major outcome of these studies for Galactic science in the near future. This makes it increasingly important to address the issues of biasing of polarization measures.

With new experiments like the *Planck* [1] satellite (Tauber et al. 2010), the balloon-borne experiments BLAST-Pol (Fissel et al. 2010) and PILOT (Bernard et al. 2007), or ground based facilities with polarization capability, such as ALMA (Pérez-Sánchez & Vlemmings 2013), SMA (Girart et al. 2006), NOEMA (at Plateau de Bure, Boissier et al. 2009), and XPOL (at the IRAM 30-m telescope, Thum et al. 2008), we are entering a new era for Galactic polarization studies, when much better control of the systematics is being achieved. Comprehensive characterization of the instrumental noise means that it becomes crucial to fully account for knowledge of the noise properties between orthogonal components when analysing these polarization measurements. Because the *Planck* data exhibit large-scale variations over the whole sky, in terms of S/N and covariance matrix, the impact of the full complexity of the noise will have to be corrected in order to obtain a uniform survey of the polarization fraction and angle – something that is essential to perform large-scale modelling of our Galaxy.

This paper is the first part of an ensemble of papers dedicated to the analysis of polarization measurements, presenting the methods for handling complex polarized data with a high level of inhomogeneity in terms of S/N or covariance matrix configurations. We aim here to present the formalism for discussing polarization fraction and angle, while taking into account the full covariance matrix. We will quantify how much the naive measurements of polarization fraction and angle are impacted by the noise covariance, and the extent to which the non-diagonal terms of the covariance matrix may be neglected. Two other studies, focused on the best estimators of the true polarization parameters, will be presented in the second and third parts of this set. Throughout, we will make use of two basic assumptions: (i) that the circular polarization (i.e., Stokes V) can be neglected; and (ii) that the noise on the other Stokes parameters can be assumed to be Gaussian.

The paper is organized as follows. We first derive in Sect. 2 the full expressions for the probability density functions of polarization fraction and angle measurements, using the full covariance matrix. In Sect. 3 we explore the impact of the complexity of the covariance matrix on polarization measurement estimates, and we provide conservative domains of the covariance matrix where the canonical simplification remains valid. We finally address the question of the S/N estimate in Sect. 4, where we compare four estimators for the polarization measurement uncertainty.

2. (p, ψ) probability density functions

2.1. Notation

The goal of this paper is to characterize the distribution of naive polarization measurements, given the true polarization parameters and their associated noise estimates. Let us denote the true values by (I_0, Q_0, U_0), representing the the true total intensity and Stokes linear polarization parameters, and with $P_0 = \sqrt{Q_0^2 + U_0^2}$. The quantities ($I$, Q, U) are the same for the measured values. The polarization fraction and polarization angle are defined by

$$p_0 \equiv \frac{\sqrt{Q_0^2 + U_0^2}}{I_0}, \quad \psi_0 \equiv \frac{1}{2}\mathrm{atan}\left(\frac{U_0}{Q_0}\right) \tag{1}$$

for the true values and

$$p \equiv \frac{\sqrt{Q^2 + U^2}}{I}, \quad \psi \equiv \frac{1}{2}\mathrm{atan}\left(\frac{U}{Q}\right) \tag{2}$$

for the measurements. The true Stokes parameters can be expressed by $Q_0 \equiv p_0\, I_0 \cos(2\psi_0)$ and $U_0 \equiv p_0\, I_0 \sin(2\psi_0)$, while for the measurements $Q \equiv p\, I \cos(2\psi)$ and $U \equiv p\, I \sin(2\psi)$. Although the true intensity I_0 is strictly positive, the measured intensity I may be negative due to noise, thus I_0 can take values between 0 and $+\infty$, while I ranges between $-\infty$ and $+\infty$. The measured Stokes parameters Q and U are real, finite quantities, spanning from $-\infty$ to $+\infty$ and with the addition of noise do not necessarily satisfy the relation $Q^2 + U^2 \leq I^2$ obeyed by the underlying quantities, i.e., $Q_0^2 + U_0^2 \leq I_0^2$. The true polarization fraction p_0 can take values in the range 0 to 1, while the measured polarization fraction p ranges between $-\infty$ and $+\infty$. Finally we define ψ_0 and ψ such that they are both defined in the range $[-\pi/2, +\pi/2]$.

Previous studies of polarization measurements usually made strong assumptions concerning the noise properties, in particular: (i) correlations between the total and polarized intensities were neglected; (ii) correlated noise between Q and U was also neglected; and (iii) equal noise was assumed on Q and U measurements. We propose instead in this paper to use the full co-

[1] *Planck* (http://www.esa.int/Planck) is a project of the European Space Agency (ESA) with instruments provided by two scientific consortia funded by ESA member states (in particular the lead countries France and Italy), with contributions from NASA (USA) and telescope reflectors provided by a collaboration between ESA and a scientific consortium led and funded by Denmark.

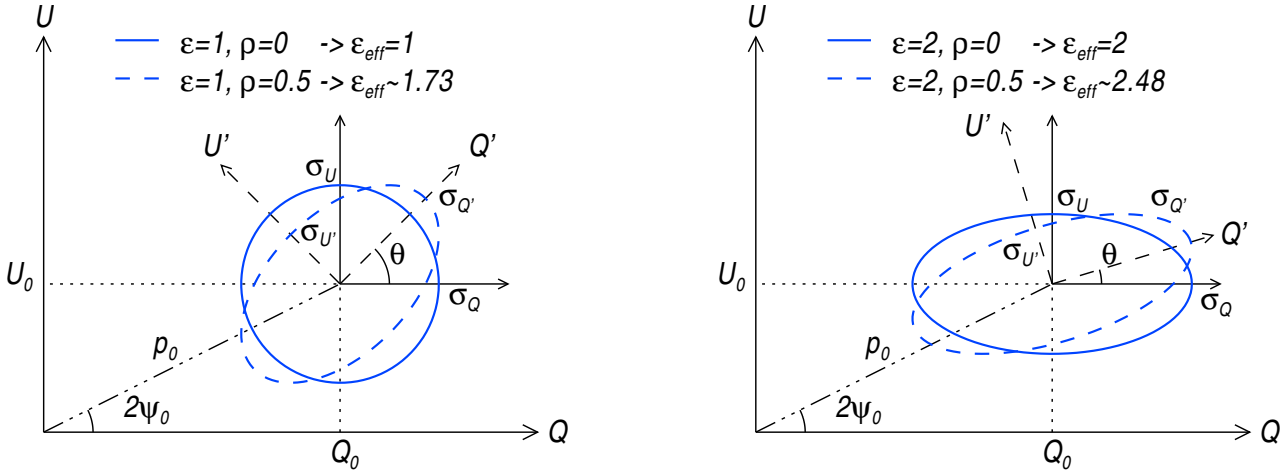

Fig. 1. Illustrations of the noise distribution in the (Q, U) plane. The blue solid and dashed lines represent the $1\,\sigma$ probability contours around the true polarization values (Q_0, U_0), also parameterized by (p_0, ψ_0). *Left*: the canonical case ($\varepsilon = 1$, $\rho = 0$) is shown as a solid line. The dashed line shows the introduction of a correlation $\rho = 0.5$, leading to an effective ellipticity ($\varepsilon_{\rm eff} > 1$) rotated by an angle θ. *Right*: same transformation, starting from the elliptical case ($\varepsilon = 2$, $\rho = 0$).

variance matrix defined by

$$\Sigma \equiv \begin{pmatrix} \sigma_{\rm II} & \sigma_{\rm IQ} & \sigma_{\rm IU} \\ \sigma_{\rm IQ} & \sigma_{\rm QQ} & \sigma_{\rm QU} \\ \sigma_{\rm IU} & \sigma_{\rm QU} & \sigma_{\rm UU} \end{pmatrix} = \begin{pmatrix} {\sigma_{\rm I}}^2 & \rho_{\rm Q}\sigma_{\rm I}\sigma_{\rm Q} & \rho_{\rm U}\sigma_{\rm I}\sigma_{\rm U} \\ \rho_{\rm Q}\sigma_{\rm I}\sigma_{\rm Q} & {\sigma_{\rm Q}}^2 & \rho\sigma_{\rm Q}\sigma_{\rm U} \\ \rho_{\rm U}\sigma_{\rm I}\sigma_{\rm U} & \rho\sigma_{\rm Q}\sigma_{\rm U} & {\sigma_{\rm U}}^2 \end{pmatrix}, \quad (3)$$

where σ_{XY} is the covariance of the two random variables X and Y, and the following quantities are usually introduced in the literature to simplify the notation:

$$\varepsilon \equiv \frac{\sigma_{\rm Q}}{\sigma_{\rm U}}; \quad \rho \equiv \frac{\sigma_{\rm QU}}{\sigma_{\rm Q}\,\sigma_{\rm U}}; \quad \rho_{\rm Q} \equiv \frac{\sigma_{\rm IQ}}{\sigma_{\rm I}\,\sigma_{\rm Q}}; \quad \rho_{\rm U} \equiv \frac{\sigma_{\rm IU}}{\sigma_{\rm I}\,\sigma_{\rm U}}. \quad (4)$$

Here ε is the ellipticity between the Q and U noise components, and ρ (which lies between -1 and $+1$) is the correlation between the Q and U noise components. Similarly $\rho_{\rm Q}$ and $\rho_{\rm U}$ are the correlations between the noise in intensity I and the Q and U components, respectively.

The parameterization just described could be misleading, however, since the ellipticity ε does not represent the effective ellipticity in the (Q, U) plane if the correlation is not null. This is illustrated in Fig. 1 for two initial values of the ellipticity ε. A new reference frame (Q', U') where the Stokes parameters are now uncorrelated can always be obtained through rotation by an angle

$$\theta = \frac{1}{2}\mathrm{atan}\left(\frac{2\sigma_{\rm QU}}{\sigma_{\rm Q}^2 - \sigma_{\rm U}^2}\right). \quad (5)$$

We can calculate the covariance matrix in the rotated frame by taking the usual $\mathsf{R}\,\Sigma\,\mathsf{R}^{\rm T}$. In this new reference frame, the errors on Q' and U' are uncorrelated and defined as

$$\begin{aligned} \sigma_{Q'}^2 &= \sigma_{\rm Q}^2\cos^2\theta + \sigma_{\rm U}^2\sin^2\theta + \sigma_{\rm QU}\sin 2\theta, \\ \sigma_{U'}^2 &= \sigma_{\rm Q}^2\sin^2\theta + \sigma_{\rm U}^2\cos^2\theta - \sigma_{\rm QU}\sin 2\theta, \end{aligned} \quad (6)$$

so that the effective ellipticity $\varepsilon_{\rm eff}$ is now given by

$$\varepsilon_{\rm eff}^2 = \frac{\sigma_{\rm Q}^2 + \sigma_{\rm U}^2 + \sigma'^2}{\sigma_{\rm Q}^2 + \sigma_{\rm U}^2 - \sigma'^2}, \quad (7)$$

where

$$\sigma'^2 = \sqrt{\left(\sigma_{\rm Q}^2 - \sigma_{\rm U}^2\right)^2 + 4\sigma_{\rm QU}^2}. \quad (8)$$

When expressed as a function of the (ε, ρ) parameters we obtain

$$\varepsilon_{\rm eff}^2 = \frac{1 + \varepsilon^2 + \sqrt{(\varepsilon^2-1)^2 + 4\rho^2\varepsilon^2}}{1 + \varepsilon^2 - \sqrt{(\varepsilon^2-1)^2 + 4\rho^2\varepsilon^2}} \quad (9)$$

and

$$\theta = \frac{1}{2}\mathrm{atan}\left(\frac{2\rho\varepsilon}{\varepsilon^2 - 1}\right). \quad (10)$$

This parameterization of the covariance matrix Σ in terms of $\varepsilon_{\rm eff}$ and θ will be preferred in our work for two reasons. Firstly, the shape of the noise distribution in the (Q, U) space is now contained in a single parameter, the effective ellipticity $\varepsilon_{\rm eff}$ (≥ 1), instead of two parameters, ε and ρ. Secondly, the noise distribution is now independent of the reference frame. This is also related to the fact that the properties of the noise distribution do not depend on 3 (I_0, p_0, ψ_0) plus 6 (from Σ) parameters, but only on 8, since it actually only depends on the difference of the angles $2\psi_0 - \theta$, which greatly simplifies the analysis. For what follows we also define $\det(\Sigma) = \sigma^6$, the determinant of the covariance matrix.

2.2. 3D probability density functions

The probability density function gives the probability to obtain a set of values (I, Q, U) given the true Stokes parameters (I_0, Q_0, U_0) and the covariance matrix Σ. As a short-hand, we refer to this as the "3D PDF." When Gaussian noise is assumed for each Stokes component, this distribution, in the space (I, Q, U) is given by

$$F(X\,|\,X_0, \Sigma) = \sqrt{\frac{\det(\Sigma^{-1})}{(2\pi)^3}}\,\exp\left(-\frac{(X - X_0)^{\rm T}\,\Sigma^{-1}\,(X - X_0)}{2}\right), \quad (11)$$

where X and X_0 are the vectors of the Stokes parameters $[I, Q, U]$ and $[I_0, Q_0, U_0]$, Σ^{-1} is the inverse of the covariance matrix (also called the "precision matrix"), and $\det(\Sigma^{-1}) = \sigma^{-6}$ is the determinant of Σ^{-1}. This definition ensures that the probability density

function is normalized to 1. Note that iso-probability surfaces in the (I, Q, U) space are ellipsoids.

Using normalized polar coordinates, the probability density function $f(I, p, \psi \,|\, I_0, p_0, \psi_0, \Sigma)$ can be computed explicitly. However, the expression (see Eq. A.1) is a little cumbersome, and so we have put it in Appendix A. Notice the presence of a factor $2|p|I^2$ in front of the exponential, coming from the Jacobian of the transformation.

2.3. 2D marginal (p, ψ) distribution

We compute the 2D probability density function $f_{2D}(p, \psi)$ by marginalizing the probability density function $f(I, p, \psi)$ (see Eq. A.1) over intensity I on the range $-\infty$ to $+\infty$. The computation is quite straightforward (see Appendix B), leading to an expression that depends on the sign of p, given in Eq. A.2 and Eq. A.3. In these expressions "erf" is the Gauss error and we have also defined the functions

$$\begin{aligned}
\alpha &= \begin{pmatrix} 1 \\ p\cos 2\psi \\ p\sin 2\psi \end{pmatrix}^{\mathrm{T}} \Sigma^{-1} \begin{pmatrix} 1 \\ p\cos 2\psi \\ p\sin 2\psi \end{pmatrix}, \\
\beta &= \begin{pmatrix} 1 \\ p\cos 2\psi \\ p\sin 2\psi \end{pmatrix}^{\mathrm{T}} \Sigma^{-1} \begin{pmatrix} 1 \\ p_0\cos 2\psi_0 \\ p_0\sin 2\psi_0 \end{pmatrix}, \\
\gamma &= \begin{pmatrix} 1 \\ p_0\cos 2\psi_0 \\ p_0\sin 2\psi_0 \end{pmatrix}^{\mathrm{T}} \Sigma^{-1} \begin{pmatrix} 1 \\ p_0\cos 2\psi_0 \\ p_0\sin 2\psi_0 \end{pmatrix}.
\end{aligned} \tag{12}$$

In many cases, two further assumptions can be made: (i) the correlations between I and (Q, U) is negligible, i.e., $\rho_{\mathrm{Q}} = \rho_{\mathrm{U}} = 0$; and (ii) the signal-to-noise ration of the intensity I_0/σ_{I} is so large that I can be considered to be perfectly known, yielding $I = I_0$. Making such assumptions allows us to reduce the covariance matrix $\bar{\Sigma}$ to a 2×2 matrix, Σ_{p}, which we define as

$$\Sigma_{\mathrm{p}} = \frac{1}{I_0^2} \begin{pmatrix} \sigma_{\mathrm{QQ}} & \sigma_{\mathrm{QU}} \\ \sigma_{\mathrm{QU}} & \sigma_{\mathrm{UU}} \end{pmatrix} = \frac{\sigma_{\mathrm{p,G}}^2}{\sqrt{1-\rho^2}} \begin{pmatrix} \varepsilon & \rho \\ \rho & 1/\varepsilon \end{pmatrix}, \tag{13}$$

where $\sigma_{\mathrm{p,G}}$ is defined by $\det(\Sigma_{\mathrm{p}}) = \sigma_{\mathrm{p,G}}^4$, leading to

$$\sigma_{\mathrm{p,G}}^2 = \frac{\sigma_{\mathrm{Q}}^2}{I_0^2} \frac{\sqrt{1-\rho^2}}{\varepsilon} \left(= \frac{\sigma_{\mathrm{Q'}}^2}{I_0^2} \frac{1}{\varepsilon_{\mathrm{eff}}} \right). \tag{14}$$

This parameter $\sigma_{\mathrm{p,G}}$ is linked to the normalization of the 2D distribution; it represents the radius of the equivalent spherical Gaussian distribution that has the same integrated area as the elliptical Gaussian distribution. The probability density function f_{2D} can then be simplified, as given in Eq. A.4. The matching between the two expressions for f_{2D}, Eqs. A.2–A.3, and Eq. A.4, when $I_0/\sigma_{\mathrm{I}} \to \infty$, is simply ensured by the consistency of the determinants of $\bar{\Sigma}$ and Σ_{p}, when $\rho_{\mathrm{Q}} = \rho_{\mathrm{U}} = 0$:

$$\sigma^6 = \sigma_{\mathrm{I}}^2 \sigma_{\mathrm{Q}}^2 \sigma_{\mathrm{U}}^2 = \sigma_{\mathrm{I}}^2 I_0^4 \sigma_{\mathrm{p,G}}^4. \tag{15}$$

We also recall that in the canonical case ($\varepsilon_{\mathrm{eff}} = 1$), the probability density function can be simplified to

$$f_{2D} = \frac{p}{\pi\sigma_{\mathrm{p}}^2} \exp\left\{ -\frac{1}{2\sigma_{\mathrm{p}}^2} \left[p^2 + p_0^2 - 2pp_0\cos 2(\psi - \psi_0) \right] \right\}, \tag{16}$$

where $\sigma_{\mathrm{p,G}}$ also simplifies to $\sigma_{\mathrm{p}} = \sigma_{\mathrm{Q}}/I_0 = \sigma_{\mathrm{U}}/I_0$. We provide illustrations of the 2D PDFs in Appendix C.

2.4. 1D Marginal p and ψ distributions

The marginal probability density functions of p and ψ can be obtained by integrating the 2D PDF given by Eq. A.4 over ψ (between $-\pi/2$ and $+\pi/2$) and p (between 0 and $+\infty$), respectively, when assuming the S/N on the intensity to be infinite. These two probability density functions theoretically depend on p_0, ψ_0, and Σ_{p}. While the expressions obtained in the general case (Aalo et al. 2007) are provided in Appendix D, the expression for the marginal p distribution reduces to the Rice law (Rice 1945) when $\varepsilon = 1$ and $\rho = 0$:

$$R(p \,|\, p_0, \sigma_{\mathrm{p}}) = \frac{p}{\sigma_{\mathrm{p}}^2} \exp\left(-\frac{(p^2 + p_0^2)}{2\sigma_{\mathrm{p}}^2} \right) \mathcal{I}_0\left(\frac{pp_0}{\sigma_{\mathrm{p}}^2} \right), \tag{17}$$

where $\mathcal{I}_0(x)$ is the zeroth-order modified Bessel function of the first kind (Abramowitz & Stegun 1964). This expression no long has a dependence on ψ_0. With the same assumptions, the marginal ψ distribution (extensively studied in Naghizadeh-Khouei & Clarke 1993) is given by

$$G(\psi \,|\, p_0, \psi_0, \sigma_{\mathrm{p}}) = \frac{1}{\sqrt{\pi}} \left\{ \frac{1}{\sqrt{\pi}} + \eta_0 e^{\eta_0^2} \left[1 + \mathrm{erf}(\eta_0) \right] \right\} e^{-p_0^2 I_0^2 / 2\sigma_{\mathrm{p}}^2}, \tag{18}$$

where $\eta_0 = (p_0 I_0 / \sqrt{2}\sigma_{\mathrm{p}}) \cos 2(\psi - \psi_0)$. This distribution depends on p_0, and is symmetric about ψ_0.

3. Impact of the covariance matrix on the bias

We now quantify how the effective ellipticity of the covariance matrix impacts the bias of the polarization measurements, compared to the canonical case. We would like to determine under what conditions the covariance matrix may be simplified to its canonical expression, in order to minimize computations. The impact of the correlation and the ellipticity of the covariance matrix are first explored in the two dimensional (p, ψ) plane with infinite intensity S/N. The cases are then investigated of finite S/N on intensity and of correlation between total and polarized intensity.

3.1. Methodology

Given a collection of measurements of the same underlying polarization parameters (p_0, ψ_0), we build the statistical bias on p and ψ by averaging the discrepancies $\Delta p = \overline{p} - p_0$ and $\Delta\psi = \overline{\psi} - \psi_0$ (always defining the quantity $\psi - \psi_0$ between $-\pi/2$ and $+\pi/2$). With knowledge of the probability density function $f_{2D}(p, \psi \,|\, p_0, \psi_0, \Sigma_{\mathrm{p}})$, we can directly obtain the statistical bias by computing the mean estimates

$$\Delta p\,(p_0, \psi_0, \Sigma_{\mathrm{p}}) = \overline{p} - p_0 \tag{19}$$

and

$$\Delta\psi\,(p_0, \psi_0, \Sigma_{\mathrm{p}}) = \overline{\psi} - \psi_0\,. \tag{20}$$

Here $\overline{p}$ and $\overline{\psi}$ are the mean estimates from the probability density function, defined as the first moments of f_{2D}:

$$\overline{p} = \int_0^{+\infty} \int_{\psi_0-\pi/2}^{\psi_0+\pi/2} p\, f_{2D}(p, \psi \,|\, p_0, \psi_0, \Sigma_{\mathrm{p}})\, dp d\psi; \tag{21}$$

and

$$\overline{\psi} = \int_0^{+\infty} \int_{\psi_0-\pi/2}^{\psi_0+\pi/2} \psi\, f_{2D}(p, \psi \,|\, p_0, \psi_0, \Sigma_{\mathrm{p}})\, dp d\psi\,. \tag{22}$$

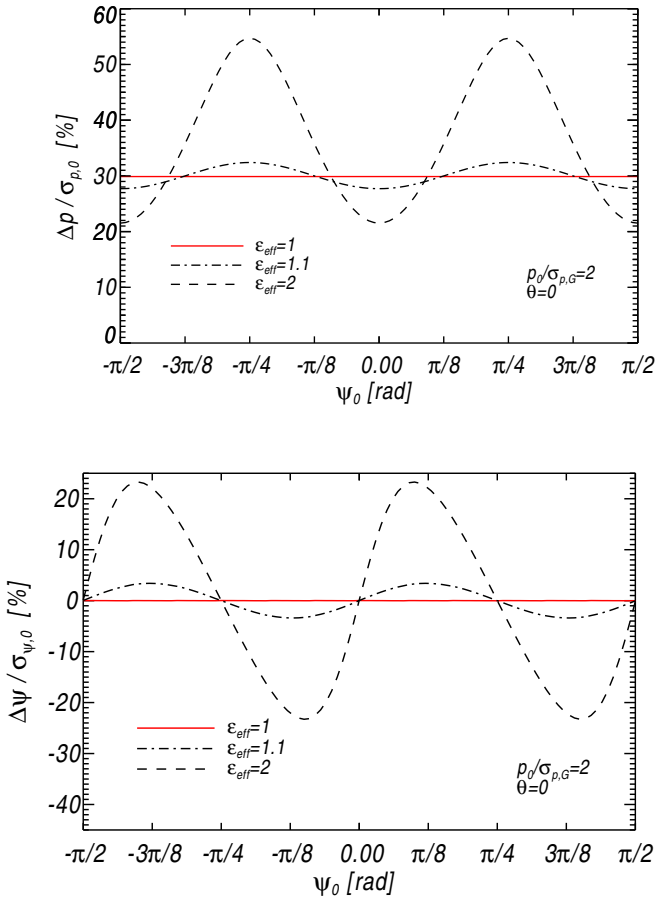

Fig. 2. Impact of the initial true polarization angle ψ_0 and varying effective ellipticity $\varepsilon_{\rm eff}$ on the relative polarization fraction bias $\Delta p/\sigma_{\rm p,0}$ (top) and the relative polarization angle bias $\Delta\psi/\sigma_{\psi,0}$ (bottom). We assume no correlation here, so that $\theta = 0$ and we set the signal-to-noise ratio to $p_0/\sigma_{\rm p,G} = 2$. The canonical case ($\varepsilon_{\rm eff} = 1$) is shown by the red line.

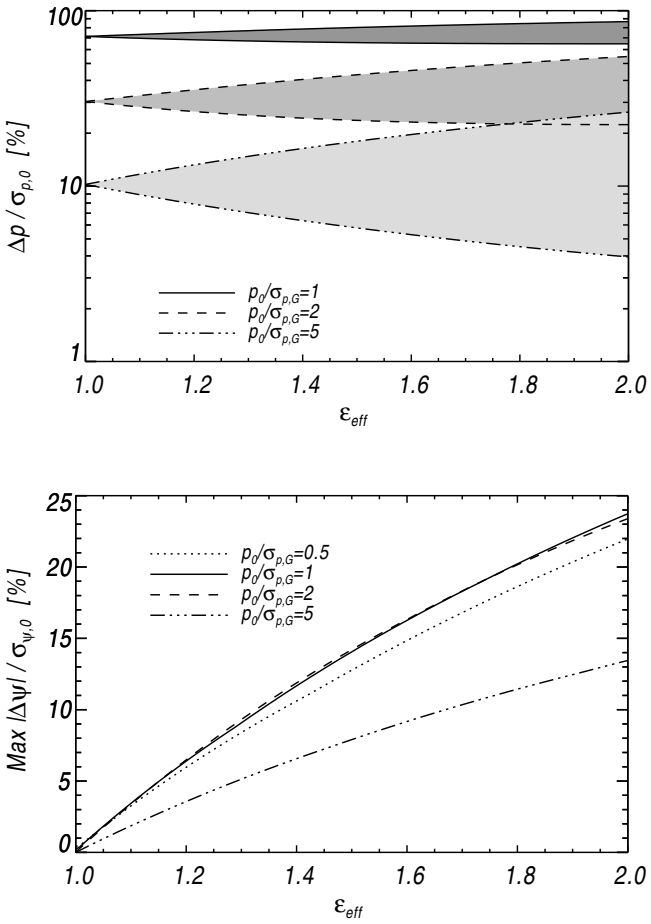

Fig. 3. Impact of the effective ellipticity $\varepsilon_{\rm eff}$ on the levels of bias. *Top*: $\Delta p/\sigma_{\rm p,0}$ as a function of the effective ellipticity $\varepsilon_{\rm eff}$, displayed for three levels of the signal-to-noise ratio, $p_0/\sigma_{\rm p,G} = 1$, 2, and 5. The grey shaded regions indicate the whole extent of variability due to ψ_0 and θ spanning the range $-\pi/2$ to $\pi/2$. *Bottom*: maximum $|\Delta\psi|/\sigma_{\psi,0}$ value for ψ_0 and θ spanning the range $-\pi/2$ to $\pi/2$, plotted as a function of the effective ellipticity $\varepsilon_{\rm eff}$, displayed for four levels of the signal-to-noise ratio, $p_0/\sigma_{\rm p,G} = 0.5$, 1, 2, and 5.

In order to quantify the importance of this bias, we can compare it to the dispersion of the polarization fraction and angle measurements, $\sigma_{p,0}$ and $\sigma_{\psi,0}$. These are defined as the second moments of the probability density function $f_{\rm 2D}$:

$$\sigma^2_{\rm p,0} = \int_0^{+\infty} \int_{-\pi/2}^{\pi/2} (p - \overline{p})^2 \, f_{\rm 2D}(p, \psi \,|\, p_0, \psi_0, \Sigma_{\rm p}) \, dp d\psi \,; \quad (23)$$

and

$$\sigma^2_{\psi,0} = \int_0^{+\infty} \int_{-\pi/2}^{\pi/2} \left(\psi - \overline{\psi}\right)^2 \, f_{\rm 2D}(p, \psi \,|\, p_0, \psi_0, \Sigma_{\rm p}) \, dp d\psi \,. \quad (24)$$

Here subscript 0 signifies that this dispersion has been computed using full knowledge of the true polarization parameters and the associated probability density function.

We choose $\sigma_{\rm p,G}$ introduced in Sect. 2.3 as our characteristic estimate of the polarization fraction noise in its relationship to the covariance matrix $\Sigma_{\rm p}$. This will be used to define the signal-to-noise ratio of the polarization fraction $p_0/\sigma_{\rm p,G}$, which is kept constant when exploring the ellipticity and correlation of the Q–U components. In Sect. 4 we will discuss how robust this estimate is against the true dispersion $\sigma_{\rm p,0}$.

We define three specific setups of the covariance matrix to investigate: (i) the *canonical* case, $\varepsilon_{\rm eff} = 1$, equivalent to $\varepsilon = 1$, $\rho = 0$; the *low* regime, $1 \leq \varepsilon_{\rm eff} < 1.1$; and the *extreme* regime, $1 \leq \varepsilon_{\rm eff} < 2$. These will be used in the rest of this paper to quantify departures of the covariance matrix from the canonical case, and to characterize the impact of the covariance matrix on polarization measurements in each regime. It is worth recalling that to each value of the effective ellipticity $\varepsilon_{\rm eff}$ there corresponds a set of equivalent parameters ε, ρ, and θ.

3.2. Q–U ellipticity

We assume here that the intensity is perfectly known and that there is no correlation between the total intensity I and the polarized intensity, so that $I = I_0$ and $\rho_{\rm Q} = \rho_{\rm U} = 0$. In this case we can now refer to Eq. A.4 for the 2D probability density function.

Contrary to the canonical case, when the effective ellipticity differs from $\varepsilon_{\rm eff} = 1$, the statistical biases on the polarization fraction and angle become dependent on the true polarization angle

ψ_0, as illustrated in Fig. 2 for the special case of $\theta = 0$ (no correlation). For extreme values of the ellipticity (e.g., $\varepsilon_{\rm eff} = 2$), the relative bias on p oscillates between 0.9 and 1.5 times the canonical bias ($\varepsilon_{\rm eff} = 1$, red line). These oscillations with ψ_0 quickly vanish when the ellipticity gets closer to 1, as shown for $\varepsilon_{\rm eff} = 1.1$ in the figure. The presence of correlations (i.e., $\rho \neq 0$) increases the effective ellipticity of the noise distribution associated with a global rotation, as detailed in sect. 2.1. Thus correlations induce the same oscillation patterns observed in Fig. 2 for a null correlation, but amplified at the corresponding effective ellipticity $\varepsilon_{\rm eff}$ and shifted by an angle $\theta/2$, according to Eqs. 9 and 10, respectively.

The top panel of Fig. 3 shows the dependence of the polarization fraction bias on the effective ellipticity for three levels of S/N: $p_0/\sigma_{\rm p,G} = 1$, 2, and 5, and including the whole range of true polarization angle ψ_0. The grey shaded regions indicate the variability interval of $\Delta p/\sigma_{\rm p,0}$ for each ellipticity, for changes in ψ_0 over the range $-\pi/2$ to $\pi/2$. We observe that the higher the S/N, the stronger the relative impact of the ellipticity compared to the canonical case. In the *low* regime the relative bias to the dispersion increases from 9% to 12% (compared to 10% in the canonical case) at a S/N of 5, while it spans from 69% and 73% (around the 71% of the canonical case) at a S/N of 1. Hence, in the *low* regime, the impact of the ellipticity on the bias of the polarization fraction represents only about 4% of the dispersion, whatever the S/N, which can therefore be neglected. However, in the *extreme* regime, the impact of the ellipticity can go up to 33% at intermediate S/N (~ 2), which can no longer be neglected.

Now concerning the impact on polarization angle – while no bias occurs in the canonical case, some oscillations in the bias $\Delta\psi$ with ψ_0 appear as soon as $\varepsilon_{\rm eff} > 1$. The amplitude can reach up to 24% of the dispersion in the *extreme* regime and up to 4% in the *low* regime, as illustrated in the bottom panel of Fig. 2. Again, these oscillations are shifted and amplified in the presence of correlations between the Stokes parameters, compared to the case with no correlation. As a global indicator, in the bottom panel of Fig. 3 we provide the maximum bias Max$|\Delta\psi|$ normalized by the dispersion $\sigma_{\psi,0}$ over the whole range of ψ_0 as a function of the ellipticity. This quantiry barely exceeds 24% (i.e., $\sim 9°$) in the worst case, i.e., for $\varepsilon_{\rm eff} = 2$ and low S/N, and it falls to below 4% (i.e., $\sim 1.5°$) in the *low* regime. Thus the bias on ψ always remains well below the level of the true uncertainty on the polarization angle at the same S/N (see Sect. 4), so that the bias of the polarization angle induced by an ellipticity $\varepsilon_{\rm eff} > 1$ can be neglected to first order for the *low* regime of the ellipticity, i.e., when there is less than a 10% departure from the canonical case.

3.3. I uncertainty

The uncertainty in the total intensity I has two sources: the measurement uncertainty expressed in the covariance matrix; and an astrophysical component of the uncertainty due to the imperfect characterization of the unpolarized contribution to the total intensity. This second source can be seen, for instance, with the cosmic infrared background in *Planck* data – its unpolarized emission can be viewed as a systematic uncertainty on the total intensity (dominated by the Galactic dust thermal emission), when one is interested in the polarization fraction of the Galactic dust. To retrieve the actual polarization fraction, it is necessary to compute it through

$$p = \frac{\sqrt{Q^2 + U^2}}{(I - \Delta I)}, \tag{25}$$

where ΔI is the unpolarized emission, which is imperfectly known. The uncertainty $\sigma_{\Delta I}$ on this quantity can be viewed as an additional uncertainty $\sigma_{\rm I}$ on the total intensity and therefore the S/N has to be written $I_0/\sigma_{\rm I} = (I - \Delta I)/\sigma_{\Delta I}$.

In order to consider the effects on polarization quantities, we first recall that, because of its definition, the measurement of polarization angle ψ is not impacted by the uncertainty on intensity (when no correlation exists between I and Q and U), contrary to the polarization fraction p, which is defined as the ratio of the polarized intensity to the total intensity. Thus the uncertainty of the total intensity does not induce any bias on ψ.

To quantify the influence of a finite signal-to-noise ratio $I_0/\sigma_{\rm I}$ on the bias of p, we compute the mean polarization fraction over the PDF:

$$\overline{p} = \iiint \frac{\sqrt{Q^2 + U^2}}{I} F\,(I, Q, U \,|\, I_0, Q_0, U_0, \mathbf{\Sigma})\, dI\, dQ\, dU, \tag{26}$$

with F given by Eq. 11. We write it this way, because using $f_{\rm 2D}$ given by Eqs. A.2 and A.3 would lead to both positive and negative logarithmic divergences for $p \to \pm\infty$ (related to samples for which $I \to 0$). These divergences can be shown to be artificial by using the Gaussian PDF of (I, Q, U) instead of $f_{\rm 2D}$.

The presence of noise in total intensity measurements increases the absolute bias $\Delta p = \overline{p} - p_0$, as shown in Fig. 4, where Δp (scaled by the true value p_0) is plotted as a function of the signal-to-noise ratio $I_0/\sigma_{\rm I}$. This is shown for three levels of the polarization S/N ratio $p_0/\sigma_{\rm p,G} = 1$, 2, and 5, and the three regimes of the covariance matrix, indicated as a solid line (*canonical*), dark shading (*low* regime) and light shading (*extreme* regime), assuming that $\rho_{\rm Q} = \rho_{\rm U} = 0$.

The absolute bias may be enhanced by a factor of 5–10 when the signal-to-noise ratio on I goes from infinite (i.e., perfectly known I) to about 2. It then drops again for lower signal-to-noise ratios, which is the result of the increasing number of negative p samples. Notice that we only consider the domain where $(I_0/\sigma_{\rm I}) > (p_0/\sigma_{\rm p,G})$.

Comparison of the bias to the dispersion $\sigma_{\rm p,0}$, as was done in the previous subsection, is not straightforward when the total intensity is uncertain. This is because the integral defining $\sigma_{\rm p,0}$ (see Eq. 23) has positive linear divergences for $p \to \pm\infty$. Unlike the case of $\overline{p}$, this divergence cannot be alleviated by working in (I, Q, U) space.

To overcome this we therefore used a proxy $\widetilde{\sigma}_{\rm p,0}$, which is the dispersion of p computed on a subset of (I, Q, U) space that excludes total intensity values below ωI_0, with $\omega = 10^{-7}$. This threshold is somewhat arbitrary, as $\widetilde{\sigma}_{\rm p,0}$ increases linearly with $1/\omega$. The value 10^{-7} is merely meant to serve as an illustration. Figure 5 shows $\Delta p/\widetilde{\sigma}_{\rm p,0}$ as a function of $I_0/\sigma_{\rm I}$ for the same values of the polarization signal-to-noise ratio $p_0/\sigma_{\rm p,G}$ and the same regimes of the covariance matrix as in Fig. 4. At high S/N for I, we asymptotically recover the values obtained in the top panel of Fig. 3. As long as $I_0/\sigma_{\rm I} > 5$, the relative bias on p is barely affected by the uncertainty on the intensity, especially for low polarization S/N, $p_0/\sigma_{\rm p,G}$. A small trend is still seen in the range $5 < I_0/\sigma_{\rm I} < 10$ for $p_0/\sigma_{\rm p,G} = 5$ – the relative bias may be enhanced by a factor of around 2 in that case, when the S/N on intensity and polarization are of the same order (~ 5). However, this situation is unlikely to be observed in astrophysical data, since the uncertainty on total intensity is usually much smaller than that on polarized intensity.

Contrary to these high S/N ($I_0/\sigma_{\rm I} > 5$) features, which are quite robust with respect to the choice of threshold ωI_0, the drop in relative bias at lower intensity S/N, i.e., $I_0/\sigma_{\rm I} < 5$, is essentially due to the divergence of the dispersion of p. Hence this part

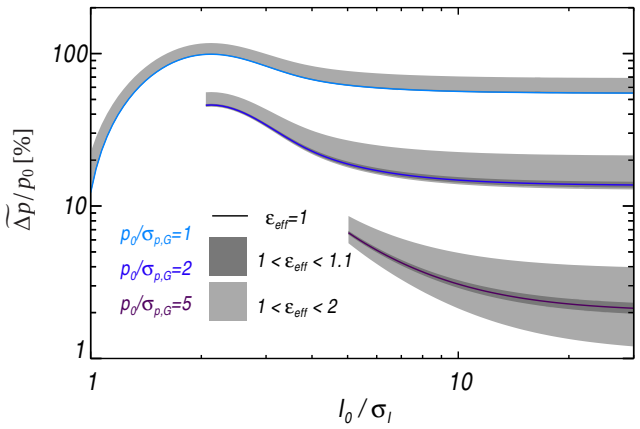

Fig. 4. Absolute polarization fraction bias normalized to the true value p_0. The level of the dispersion scaled to the true value, $\sigma_{\rm p,0}/p_0$, is shown as a dashed line for the canonical case as a function of the S/N $I_0/\sigma_{\rm I}$, plotted for three values of the polarization S/N, $p_0/\sigma_{\rm p,G}$, and values of the effective ellipticity $\varepsilon_{\rm eff}$ covering the *canonical*, *low*, and *extreme* regimes of the covariance matrix. The intensity correlation coefficients are set to $\rho_{\rm Q}=\rho_{\rm U}=0$. Notice that we only consider the domain where $(I_0/\sigma_{\rm I})>(p_0/\sigma_{\rm p,G})$.

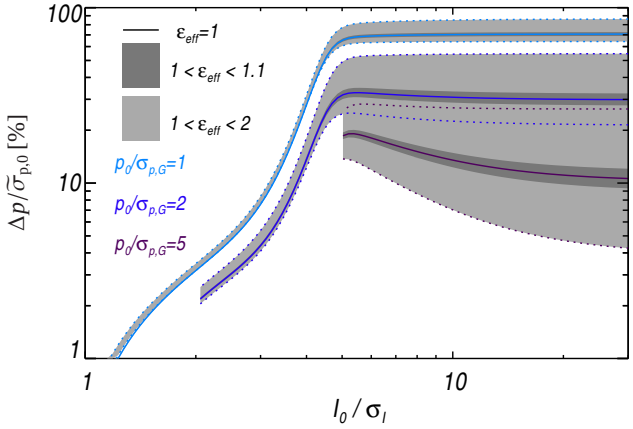

Fig. 5. Same as Fig. 4, but showing the bias on the polarization fraction relative to the dispersion proxy $\widetilde{\sigma}_{\rm p,0}$. See text for a description of this quantity.

of Fig. 4 should be taken as nothing more than an illustration of the divergence at low S/N for I. It should be stressed, however, that this increase of the dispersion of p has to be carefully taken into account when dealing with low S/N intensity data, which can be the case well away from the Galactic plane.

3.4. Correlation between I and Q–U

With non-zero noise on total intensity, it becomes possible to explore the effects of the coefficients $\rho_{\rm Q}$ and $\rho_{\rm U}$, corresponding to correlation between the intensity I and the (Q,U) plane.

We first note that the introduction of correlation parameters $\rho_{\rm Q}$ and $\rho_{\rm U}$ that are different from zero directly modifies the ellipticity ε and correlation ρ between Stokes Q and U. Simple considerations on the Cholesky decomposition of the covariance matrix $\mathbf{\Sigma}$ (given in Appendix E) show that for a given ellipticity ε and correlation parameter ρ, obtained when $\rho_{\rm Q}=\rho_{\rm U}=0$, the ellipticity ε' and correlation ρ' become

$$\varepsilon' = \varepsilon\sqrt{\frac{1-\rho_{\rm Q}^2}{1-\rho_{\rm U}^2}} \quad \text{and} \quad \rho' = \rho_{\rm Q}\rho_{\rm U} + \rho\sqrt{\left(1-\rho_{\rm Q}^2\right)\left(1-\rho_{\rm U}^2\right)} \tag{27}$$

when $\rho_{\rm Q}$ and $\rho_{\rm U}$ are no longer null. Consequently, non null $\rho_{\rm Q}$ and $\rho_{\rm U}$ yield similar impacts as found for a non-canonical effective ellipticity ($\varepsilon_{\rm eff}\neq1$), discussed in Sect. 3.2. Moreover, in order to investigate the sole impact of non-null $\rho_{\rm Q}$ and $\rho_{\rm U}$ with a finite S/N on the intensity, we have compared the case $(\varepsilon,\rho,\rho_{\rm Q},\rho_{\rm U})$ to the reference case $(\varepsilon',\rho',0,0)$. We find that the relative change of the polarization fraction bias Δp is at most 10–15% over the whole range of $I_0/\sigma_{\rm I}$ explored in this work (i.e., $I_0/\sigma_{\rm I}\geqslant1$).

Concerning the polarization angle bias, the difference between the bias computed for $(\varepsilon,\rho,\rho_{\rm Q},\rho_{\rm U})$ and that for the reference case $(\varepsilon',\rho',0,0)$ is at most $\Delta\psi-\Delta\psi_{\rm ref}\sim4°$, and essentially goes to zero above $I_0/\sigma_{\rm I}\sim2$–3. The dependence of the change in bias with $(\rho_{\rm Q},\rho_{\rm U})$ is similar to that for $\Delta p/\Delta p_{\rm ref}$, except that it depends solely on $\rho_{\rm U}$ for $\psi_0=0$ and solely on $\rho_{\rm Q}$ for $\psi_0=\pi/4$.

4. Polarization uncertainty estimates

If we are given the polarization measurements and the noise covariance matrix of the Stokes parameters, we would like to derive estimates of the uncertainties associated with the polarization fraction and angle. These are required to: (i) define the signal-to-noise ratio of these polarization measurements; and (ii) quantify how important the bias is compared to the accuracy of the measurements. In the most general case the uncertainties in the polarization fraction and angle do not follow a Gaussian distribution, so that confidence intervals should be properly used to obtain an estimate of the associated errors, as is described in Sec. 4.5. However, it can sometimes be assumed as a first approximation that the distributions are Gaussian, in order to derive quick estimates of the p and ψ uncertainties, defined as the variance of the 2D distribution of the polarization measurements. We explore below the extent to which this approximation can be utilized, when using the most common estimators of these two quantities.

4.1. Standard deviation estimates

To compare the robustness of the uncertainty estimates, we build 10 000 Monte Carlo simulated measurements in each of the three regimes of the covariance matrix (*canonical*, *low*, and *extreme*), by varying the S/N of p and the polarization angle ψ_0 inside the range $-\pi/2$ and $\pi/2$. We use the simulations to compute the posterior fraction of measurements for which the true value p_0 or ψ_0 falls inside the $\pm\sigma$ range around the measurement. This provides the probability $\mathcal{P}$ shown in Figs. 6 and 7, for p and ψ, respectively.

We first focus on the true uncertainty estimates, as defined in Sect. 3.1. We observe that the $\sigma_{\rm p,0}$ true estimates (top left of Fig. 6) fall below the Gaussian value erf($\sqrt{2}/2$) (i.e., 68%) once the S/N goes below 3. The $\sigma_{\psi,0}$ true estimates (left of Fig. 7) provide conservative probabilities ($\mathcal{P}>68\%$) for S/N > 0.5. This is also shown in Fig. 8 as a function of the S/N, for the *canonical*, *low*, and *extreme* regimes of the covariance matrix. Notice that it is not strongly dependent on the ellipticity of the covariance matrix. It shows a maximum of $\pi/\sqrt{12}\simeq52°$ at low S/N, and converges slowly to 0 at high S/N (still being $\sim10°$ at a S/N = 3). Thus we might imagine using such estimates as reasonably good

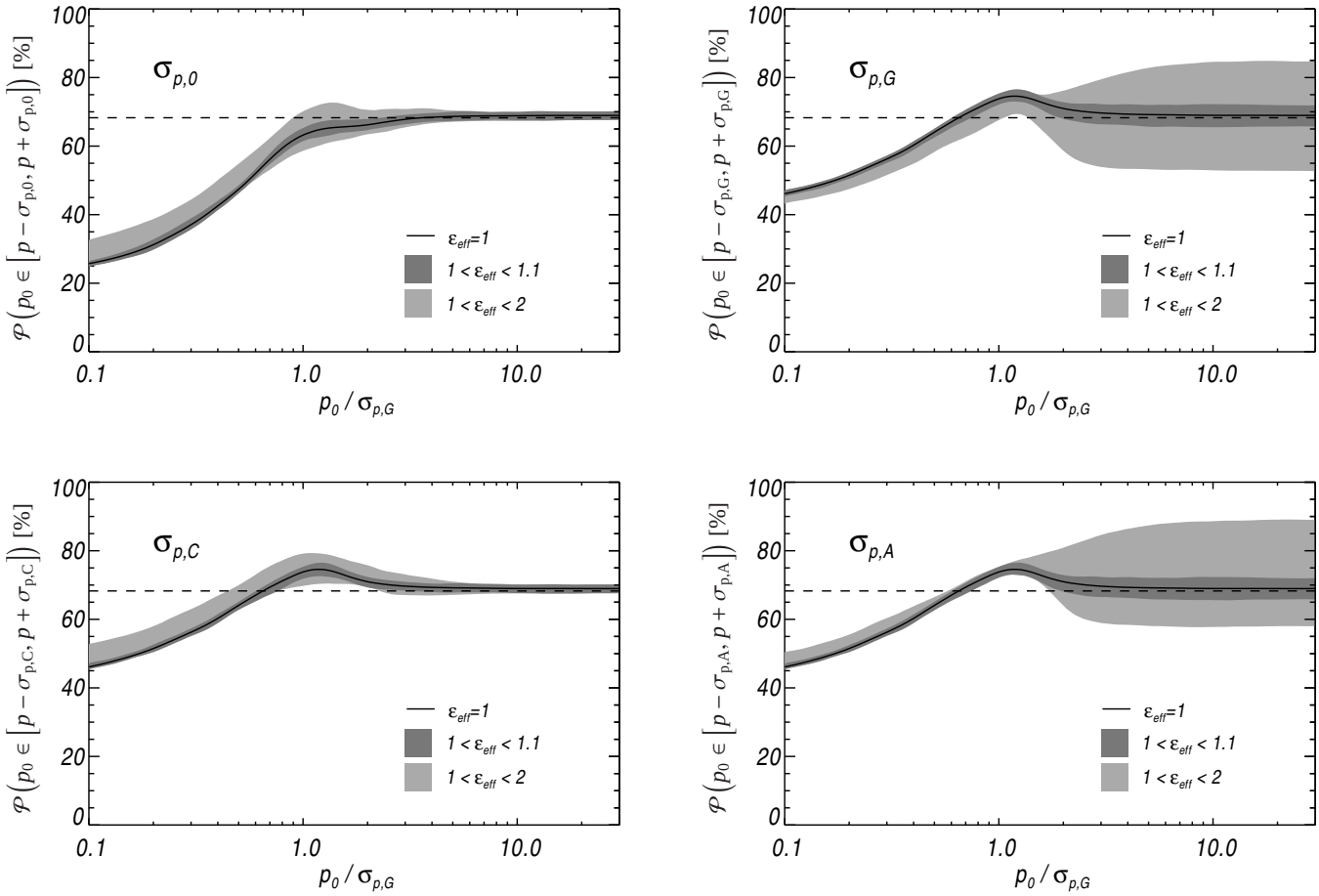

Fig. 6. Probability $\mathcal{P}$ to find the true polarization fraction p_0 inside the interval $[p - \sigma_{\rm p}^{\rm low}, p + \sigma_{\rm p}^{\rm up}]$, where $\sigma_{\rm p}^{\rm low}$ and $\sigma_{\rm p}^{\rm up}$ are the $1\,\sigma$ lower and upper limits, respectively. We plot this for each estimators: true $\sigma_{\rm p,0}$ (top left); classical $\sigma_{\rm p,C}$ (bottom left); geometric $\sigma_{\rm p,G}$ (top right); and arithmetic $\sigma_{\rm p,A}$ (bottom right). These are plotted as a function of the S/N $p_0/\sigma_{\rm p,G}$. Monte Carlo simulations have been carried out in the *canonical* (solid line), *low* (dark grey), and *extreme* (light grey) regimes of the covariance matrix. The expected 68.27% level is shown as a dashed line.

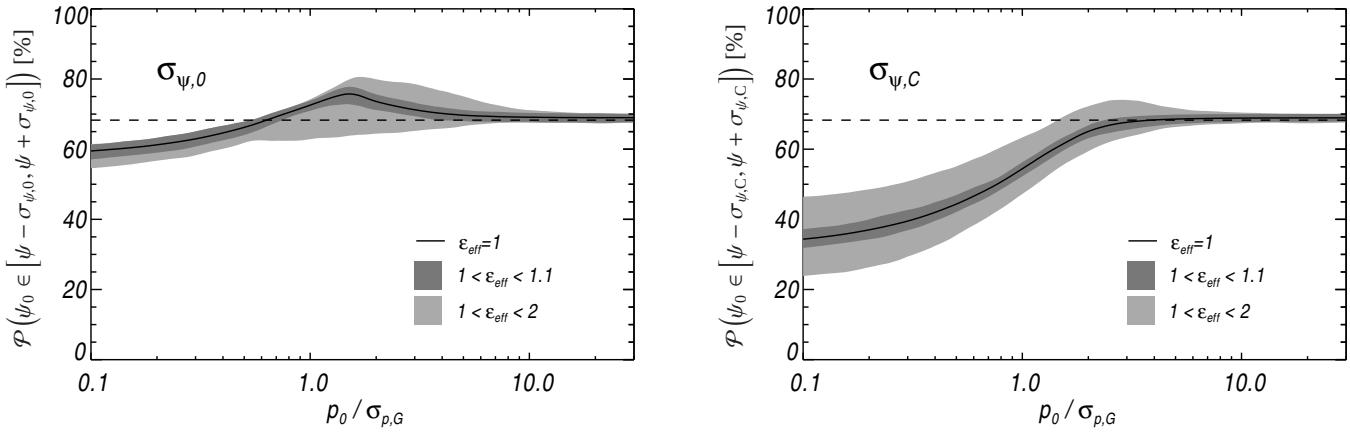

Fig. 7. Same as Fig. 6, but for the polarization angle uncertainty estimators. *Left*: $\sigma_{\psi,0}$. *Right*: classical $\sigma_{\psi,\rm C}$.

approximations to the uncertainties at high S/N (> 3) for p, and over almost the entire range of S/N for ψ. However, these true p and ψ uncertainties, $\sigma_{\rm p,0}$ and $\sigma_{\psi,0}$, respectively, depend on p_0 and ψ_0, which remain theoretically unknown. Thus we can only provide specific estimates of those variance quantities, as detailed below.

4.2. Geometric and arithmetic estimators

Two estimates of the polarization fraction uncertainty can be obtained independently of the measurements themselves, which makes them easy to compute: (i) the geometric ($\sigma_{\rm p,G}$) estimate; and (ii) the arithmetic ($\sigma_{\rm p,A}$) estimate.

The geometric estimator was already introduced earlier, when we derived the expression for the two dimensional (p, ψ) probability density function $f_{\rm 2D}$. It is defined via the determinant of the 2D covariance matrix $\mathbf{\Sigma}_{\rm p}$ as $\det(\mathbf{\Sigma}_{\rm p}) = \sigma^4_{\rm p,G}$, with its expression given in Eq. 14. We recall that the determinant of the covariance matrix $\mathbf{\Sigma}_{\rm p}$ is linked to the area inside a probability contour, and independent of the reference frame of the Stokes parameters. In the canonical case, this estimate gives back the usual expressions, $\sigma_{\rm p,G} = \sigma_{\rm Q}/I_0 = \sigma_{\rm U}/I_0$, used to quantify the noise on the polarization fraction. It can be considered as the geometric mean of $\sigma_{\rm Q}$ and $\sigma_{\rm U}$ when there is no correlation between them, i.e., $\sigma^2_{\rm p,G} = \sigma_{\rm Q}\sigma_{\rm U}/I_0^2$.

The arithmetic estimator is defined as a simple quadratic mean of the variance in Q and U:

$$\sigma^2_{\rm p,A} = \frac{1}{2}\frac{\sigma^2_{\rm Q} + \sigma^2_{\rm U}}{I_0^2} = \frac{\sigma^2_{\rm Q}}{I_0^2}\frac{(\varepsilon^2+1)}{2\varepsilon^2}. \tag{28}$$

This estimate also gives back $\sigma_{\rm p,A} = \sigma_{\rm Q}/I_0 = \sigma_{\rm U}/I_0$ in the canonical case. Furthermore, it is also independent of the reference frame or whether correlations are present.

The two estimators have very similar behaviour, as can be seen in the top and bottom right panels of Fig. 6. They agree perfectly with a 68% confidence level for S/N $p_0/\sigma_{\rm p,0} > 4$ and for standard simplification of the covariance matrix. Both estimators provide conservative probability ($\mathcal{P}$, > 68%) in the S/N range 0.5-4. The impact of the effective ellipticity of the covariance matrix (grey shaded area) is stronger for larger values of the S/N (>2), and can yield variations of 30% in the probability $\mathcal{P}$ for the *extreme* regime. These estimators should be used cautiously for high ellipticity, but provide quick and conservative estimates in the other cases.

4.3. Classical Estimate

The classical determination of the uncertainties proposed by Serkowski (1958, 1962) is often used for polarization determinations based on optical extinction data. Although investigated by Naghizadeh-Khouei & Clarke (1993), these classical uncertainties still do not include asymmetrical terms and correlations in the covariance matrix. Here we extend the method to the general case, by using the derivatives of p and ψ around the observed values of the I, Q, and U parameters. It should be noted that, since this approach is based on derivatives around the observed values of (I, Q, U), it is only valid in the high signal-to-noise regime. The detailed derivation, provided in Appendix F, leads to the expressions

$$\sigma^2_{\rm p,C} = \frac{1}{p^2 I^4} \times \Big(Q^2\sigma^2_{\rm Q} + U^2\sigma^2_{\rm U} + p^4 I^2 \sigma^2_{\rm I} + 2QU\sigma_{\rm QU} - 2IQp^2\sigma_{\rm IQ} - 2IUp^2\sigma_{\rm IU}\Big) \tag{29}$$

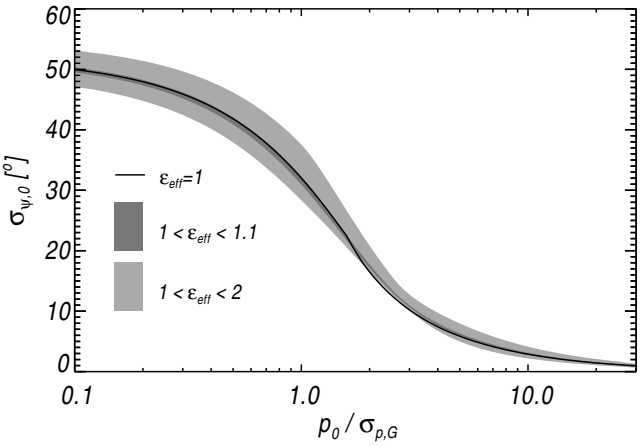

Fig. 8. True polarization angle uncertainty, $\sigma_{\psi,0}$, as a function of the S/N, $p_0/\sigma_{\rm p,G}$. The three regimes (*canonical*, *low*, and *extreme*) of the covariance matrix are explored (solid line, light, and dark grey shaded regions, respectively).

and

$$\sigma^2_{\psi,\rm C} = \frac{1}{4}\frac{Q^2\sigma^2_{\rm U} + U^2\sigma^2_{\rm Q} - 2QU\sigma_{\rm QU}}{(Q^2+U^2)^2}\ \text{rad}^2, \tag{30}$$

where I, Q, U, and p are the measured quantities, and σ_{XY} are the elements of the covariance matrix. We recall that the maximum uncertainty on ψ is equal to $\pi/\sqrt{12}$ rad (integral of the variance of the polarization angle over a flat distribution between $-\pi/2$ and $\pi/2$). When $\sigma_{\rm I}$ can be neglected, we obtain

$$\sigma_{\psi,\rm C} = \sqrt{\frac{Q^2\sigma^2_{\rm U} + U^2\sigma^2_{\rm Q} - 2QU\sigma_{\rm QU}}{Q^2\sigma^2_{\rm Q} + U^2\sigma^2_{\rm U} + 2QU\sigma_{\rm QU}}} \times \frac{\sigma_{\rm p,C}}{2p}\ \text{rad}. \tag{31}$$

Because the uncertainty of ψ is also often expressed in degrees, we provide the associated conversions: $\pi/\sqrt{12}\,\text{rad} = 51.^\circ96$; and $1/2\,\text{rad} = 28.^\circ65$. Moreover, under the canonical assumptions, we recover $\sigma_{\rm p,C} = \sigma_{\rm p,G} = \sigma_{\rm Q}/I_0 = \sigma_{\rm U}/I_0$ and $\sigma_{\psi,\rm C} = \sigma_{\rm p,C}/2p$ rad.

Since the classical estimate of the uncertainty $\sigma_{\rm p,C}$ is equal to $\sigma_{\rm p,G}$ under the standard simplifications of the covariance matrix, it has the same deficiency at low S/N (see bottom left panel of Fig. 6). The impact of the effective ellipticity of the covariance matrix (grey shaded area) tends to be negligible at high S/N ($p_0/\sigma_{\rm p,G} > 4$), and remains limited at low S/N. Thus this estimator of the polarization fraction uncertainty appears more robust than the geometric and arithmetic estimators, while still being easy to compute, and valid (even conservative) over a wide range of S/N.

The classical estimate of the polarization angle uncertainty, $\sigma_{\psi,\rm C}$, is shown in Fig. 7 (right panel) in the *canonical*, *low*, and *extreme* regimes of the covariance matrix. It appears that $\sigma_{\psi,\rm C}$ is strongly under-estimated at low S/N, mainly due to the presence of the term $1/p$ in Eq. 31, where p is strongly biased at low S/N. For S/N > 4, the agreement between the probability $\mathcal{P}$ and the expected value is good, while the impact of the ellipticity of the covariance matrix becomes negligible only for S/N > 10. Hence this estimator can cetainly be used at high S/N.

4.4. S/N estimates

It is important to stress how any measurement of the signal-to-noise ratio, $p/\sigma_{\rm p,G}$, is highly impacted by the bias on the mea-

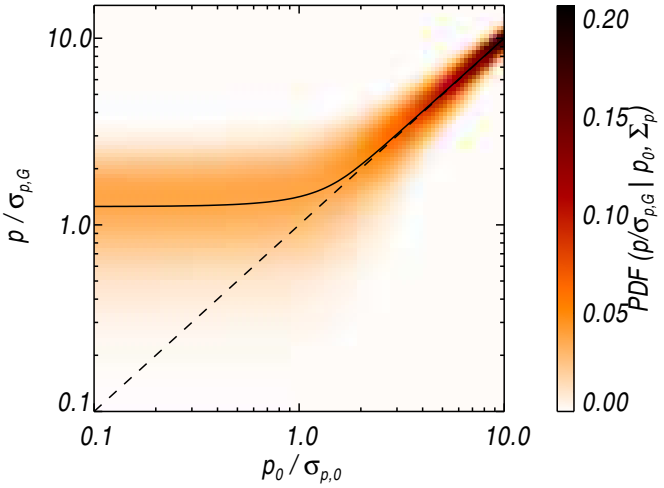

Fig. 9. Probability density function of the measured signal-to-noise ratio $p/\sigma_{\rm p,G}$ (where $\sigma_{\rm p,G}$ is the geometric estimate) as a function of the true signal-to-noise ratio $p_0/\sigma_{\rm p,0}$, with no ellipticity and correlation in the covariance matrix $\Sigma_{\rm p}$. The mean likelihood, $\overline{p}/\sigma_{\rm p,G}$ (full line), tends to $\sqrt{\pi/2}$ at low S/N and to the 1:1 relation (dashed line) at high S/N ($p_0/\sigma_{\rm p,0} > 2$).

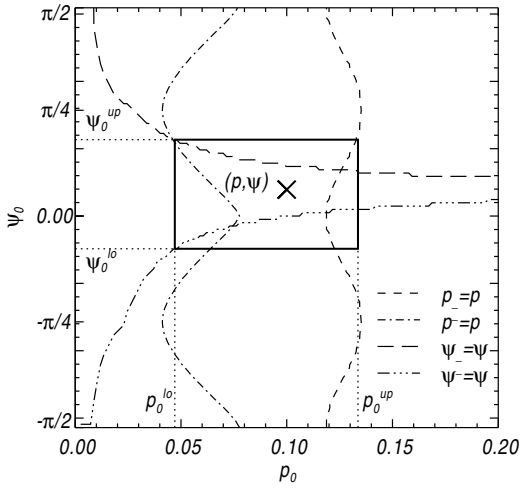

Fig. 10. Construction of 68% confidence intervals $[p_0^{\rm low}, p_0^{\rm up}]$ and $[\psi_0^{\rm low}, \psi_0^{\rm up}]$ (full line box) of p_0 and ψ_0, based on the upper and lower loci $p = p_-$, $p = p^-$, $\psi = \psi_-$, and $\psi = \psi^-$, built from probability density functions $f_{\rm 2D}$ and a given measurement (p, ψ) (indicated by the cross).

sured polarization fraction p, as shown in Fig. 9. We observe that at high S/N ($p_0/\sigma_{\rm p,0} > 2$) the measured S/N, here $p/\sigma_{\rm p,G}$, is very close to the true S/N (dashed line). The mean likelihood of the measured S/N (solid line) flattens for lower true S/N, such that $\overline{p}/\sigma_{\rm p,G}$ tends to $\sqrt{\pi/2}$ for $p_0/\sigma_{\rm p,0} < 1$, which comes from the limit of the Rice (1945) function when $p_0/\sigma_{\rm p,0} \to 0$. This should be taken into account carefully when dealing with polarization measurements at intermediate S/N. For any measurement with a S/N $p_0/\sigma_{\rm p,0} < 2$, it is in fact impossible to obtain an estimate of the true S/N, because this is fully degenerate due to the bias of the polarization fraction.

4.5. Confidence intervals

We have seen the limitations of the Gaussian assumption for computing valid estimates of the polarization uncertainties. To obtain a robust estimate of the uncertainty in p and ψ at low S/N, one has to construct the correct confidence regions or intervals. The λ % confidence interval around a measurement p is defined as the interval which has a probability of containing the true value p_0 exactly equal to $\lambda/100$, where $(1-\lambda)$ is called "critical parameter." This interval is constructed from the probability density function and does not require any estimate of the true polarization parameters. Mood & Graybill (1974), Simmons & Stewart (1985) and Vaillancourt (2006) provided a simple way to construct such confidence intervals for the polarization fraction p when the usual simplifications of the covariance matrix are assumed. Naghizadeh-Khouei & Clarke (1993) have provided estimates of the confidence intervals for the polarization angle ψ under similar assumptions, and this is even simpler, because in that case $f_\psi(\psi \mid p_0, \psi_0, \Sigma_{\rm p})$ only depends on the signal-to-noise ratio $p_0/\sigma_{\rm p,0}$.

Once the covariance matrix is allowed to include ellipticity and correlations, we have seen in Sect. 2.4 and Appendix D how the marginalized probability density functions $f_{\rm p}(p \mid p_0, \psi_0, \Sigma_{\rm p})$ and $f_\psi(\psi \mid p_0, \psi_0, \Sigma_{\rm p})$ depend on the true polarization fraction p_0 and the true polarization angle ψ_0. This leads is to consider ψ_0 as a "nuisance parameter" when building confidence intervals of p_0, and vice-versa. We propose below an extension of the Simmons & Stewart (1985) technique, using an iterative method to build the confidence intervals of p_0 and ψ_0 simultaneously.

For each possible value of p_0 and ψ_0 (spanning the range 0 to 1, and $-\pi/2$ to $\pi/2$, respectively), we compute the quantities p_-, p^-, ψ_- and ψ^-, which provide the lower and upper limits in p and ψ of the region $\Omega(\lambda, p_0, \psi_0)$ defined by

$$\iint_{\Omega(\lambda,p_0,\psi_0)} f_{\rm 2D}(p, \psi \mid p_0, \psi_0, \Sigma_{\rm p})\, dp d\psi = \frac{\lambda}{100} \qquad (32)$$

and such that the contour of the region Ω is an iso-probability contour of the probability density function $f_{\rm 2D}$. We stress that the choice of a confidence interval is still subjective and may be shifted by any arbitrary value of p or ψ, provided that the integral over the newly defined region is also $\lambda/100$. The definition we have chosen ensures that the region $\Omega(\lambda, p_0, \psi_0)$ is the smallest possible. We also note that

$$\int_{p_-}^{p^-} \int_{\psi_-}^{\psi^-} f_{\rm 2D}\, dp d\psi > \iint_{\Omega(\lambda,p_0,\psi_0)} f_{\rm 2D}\, dp d\psi, \qquad (33)$$

which implies that the rectangular region bounded by p_-, p^-, ψ_- and ψ^- is a conservative choice. For a given λ and covariance matrix $\Sigma_{\rm p}$, we can finally obtain a set of four upper and lower limits on p and ψ: $p_-(p_0, \psi_0)$; $p^-(p_0, \psi_0)$; $\psi_-(p_0, \psi_0)$; and $\psi^-(p_0, \psi_0)$. We illustrate this with the example of (p, ψ) set to $(0.1, \pi/8)$ in Fig. 10 (this point shown by the cross). For given polarization measurements (p, ψ), we trace the loci $p_-(p_0, \psi_0) = p$ (dashed line), $p^-(p_0, \psi_0) = p$ (dot-dash line), $\psi_-(p_0, \psi_0) = \psi$ (long dashed line), and $\psi^-(p_0, \psi_0) = \psi$ (dash-dot-dot-dot line). Finally, the 68% confidence intervals $[p_0^{\rm low}, p_0^{\rm up}]$ of p_0 and $[\psi_0^{\rm low}, \psi_0^{\rm up}]$ of ψ_0 are defined by building the smallest rectangular region (solid line in Fig. 10) that simultaneously covers the domain in p_0 and ψ_0 between the upper and lower limits de-

fined above, and which satisfies the conditions:

$$\begin{aligned} p_0^{\rm low} &= \min_{p_0}\left(p = p^- \left\{ p_0\ ,\ \psi_0 \in [\psi_0^{\rm low}, \psi_0^{\rm up}] \right\} \right); \\ p_0^{\rm up} &= \max_{p_0}\left(p = p_- \left\{ p_0\ ,\ \psi_0 \in [\psi_0^{\rm low}, \psi_0^{\rm up}] \right\} \right); \\ \psi_0^{\rm low} &= \min_{\psi_0}\left(\psi = \psi^- \left\{ p_0 \in [p_0^{\rm low}, p_0^{\rm up}]\ ,\ \psi_0 \right\} \right); \\ \psi_0^{\rm up} &= \max_{\psi_0}\left(\psi = \psi_- \left\{ p_0 \in [p_0^{\rm low}, p_0^{\rm up}]\ ,\ \psi_0 \right\} \right). \end{aligned} \quad (34)$$

Using these conditions, the confidence interval of p_0 takes into account the nuisance parameter ψ_0 over its own confidence interval, and vice-versa. This has to be constructed iteratively, starting with $\psi_0^{\rm low} = -\pi/2$ and $\psi_0^{\rm up} = \pi/2$, to build first guesses for $p_0^{\rm low}$ and $p_0^{\rm up}$, which are then used to build a new estimate of the confidence intervals of ψ_0, and so on until convergence. In practice, it converges very quickly. We emphasize that these confidence intervals are conservative, because they include the impact of the nuisance parameters, implying that

$$\Pr\left(p_0^{\rm low} \le p_0 \le p_0^{\rm up}\ ;\ \psi_0^{\rm low} \le \psi_0 \le \psi_0^{\rm up}\right)\Big|_{p,\psi,\Sigma_{\rm p}} \ge \frac{\lambda}{100} \quad (35)$$

whatever the true values p_0, ψ_0.

5. Conclusions

This paper represents the first step in an extensive study of polarization analysis methods. We focused here on the impact of the full covariance matrix on naive polarization measurements, and especially the impact on the bias. We have derived analytical expressions for the probability density function of the polarization parameters (I, p, ψ) in the 3D and 2D cases, taking into account the full covariance matrix $\mathbf{\Sigma}$ of the Stokes parameters I, Q, and U.

The asymmetries of the covariance matrix can be characterized by the effective ellipticity $\varepsilon_{\rm eff}$, expressed as a function of the ellipticity ε and the correlation ρ between Q and U in a given reference frame, and by the correlation parameters $\rho_{\rm Q}$ and $\rho_{\rm U}$ between the intensity I and the Q and U parameters. We have quantified departures from the canonical case ($\varepsilon_{\rm eff} = 1$), usually assumed in earlier works on polarization. We explored this effect for three regimes of the covariance matrix: the *canonical* case, $\varepsilon_{\rm eff} = 1$); the *low* regime, $1 < \varepsilon_{\rm eff} < 1.1$; and the *extreme* regime $1 < \varepsilon_{\rm eff} < 2$. We first emphasized the impact of the true polarization angle ψ_0, which can produce variations in the polarization fraction bias of up to 30% of the dispersion of p, in the *extreme* regime, and up to 5% in the *low* regime. We then estimated the statistical bias on the polarization angle measurement ψ. This can reach up to 9° when the ellipticity or the correlation between the Q and U Stokes components becomes important ($\varepsilon_{\rm eff} \sim 2$), and the S/N is low. However, when values of the effective ellipticity are in the *low* regime (i.e., less than 10% greater than the canonical values) the bias on ψ remains limited (i.e., $< 1°$), and well below (by a factor of 5–25) the level of the measurement uncertainty. Thus the bias on ψ can be neglected, to first order, for small departures of the covariance matrix from the canonical case.

On the other hand, we have quantified the impact of the uncertainty of the intensity on the relative and absolute statistical bias of the polarization fraction and angle. We provided the modified probability density function in (p, ψ) arising from a finite signal-to-noise ratio of the intensity, $I_0/\sigma_{\rm I}$. We have shown that, above an intensity S/N of 5, the relative bias on the polarization fraction p remains globally unchanged at polarization S/N $p_0/\sigma_{\rm p,G} < 2$, while it is slightly enhanced when the intensity and the polarization S/N lie in the intermediate range, $p_0/\sigma_{\rm p,G} > 2$. For S/N on the intensity $I_0/\sigma_{\rm I}$ below 5, the relative bias on p drops suddenly to 0, because of the increasing dispersion. Indeed, the absolute bias can be higher by a factor as large as 5 when the S/N on I drops below 2 to 3; this is associated with a dramatical increase in the dispersion of the polarization fraction, which diverges and strongly overwhelms the increase of the bias at low S/N. Hence the uncertainty of the intensity has to be properly taken into account when analysing polarization data for faint objects, in order to derive the correct polarization fraction bias and uncertainty. Similarly, the case of faint polarized objects on top of a varying but unpolarized background can lead to a question about the correct intensity offset to subtract, yielding an effective additional uncertainty on the intensity.

The impact of correlations between the intensity and the Q and U components has also been quantified in the case of a finite S/N on the intensity. It has been shown that the bias on p is only slightly affected (below 10% difference compared with the canonical case) even at low S/N on I, when the correlations $\rho_{\rm Q}$ and $\rho_{\rm U}$ span the range −0.2 to 0.2.

We have additionally addressed the question of how to obtain a robust estimate of the uncertainties on polarization measurements (p, ψ). We extended the often used procedure of Simmons & Stewart (1985) by building confidence intervals for polarization fraction and angle simultaneously, taking into account the full properties of the covariance matrix. This method makes it possible to build conservative confidence intervals around polarization measurements.

We have explored the domain of validity for the commonly used polarization uncertainty estimators based on the variance of the probability density function (assuming a Gaussian distribution). The true dispersion of the polarization fraction has been shown to provide robust estimates only at high S/N (above 3), while the true dispersion of the polarization angle yields conservative estimates for S/N > 0.5. Simple estimators, such as the geometric and arithmetic polarization fraction uncertainties, appear sensitive to the effective ellipticity of the covariance matrix at high S/N, while they provide conservative estimates over a wide range of S/N (above 0.5) in the canonical case. The classical method, usually adopted to analyse optical extinction polarization data, provides the most robust estimates of $\sigma_{\rm p}$ for S/N above 0.5, with respect to the ellipticity of the covariance matrix, but poor estimates of σ_ψ, which are valid only at very high S/N (above 5).

We have seen how much the naive polarization estimates provide poor determinations of the true polarization parameters, and how it can be difficult to recover the true S/N of a measurement. In a companion paper (Montier et al. in preparation), we review different estimators of the true polarization from experimental measurements that partially correct this bias in p and ψ, using full knowledge of the polarization covariance matrix.

Acknowledgements. This paper was developed to support the analysis of data from the *Planck* satellite. The development of *Planck* has been supported by: ESA; CNES and CNRS/INSU-IN2P3-INP (France); ASI, CNR, and INAF (Italy); NASA and DoE (USA); STFC and UKSA (UK); CSIC, MICINN, JA, and RES (Spain); Tekes, AoF, and CSC (Finland); DLR and MPG (Germany); CSA (Canada); DTU Space (Denmark); SER/SSO (Switzerland); RCN (Norway); SFI (Ireland); FCT/MCTES (Portugal); and PRACE (EU). A description of the Planck Collaboration and a list of its members, including the technical or scientific activities in which they have been involved, can be found at http://www.sciops.esa.int/index.php?project=planck&page=Planck_Collaboration. We acknowledge the use of the Legacy Archive for Microwave Background Data Analysis (LAMBDA), part of the High Energy Astrophysics Science Archive Center (HEASARC). HEASARC/LAMBDA is a service of the Astrophysics Science Division at the NASA Goddard Space Flight Center. Some of the results in this paper have been derived using the HEALPix

package. We would also like to thank P. Leahy, S. Prunet and D. Scott for their very useful comments.

References

Aalo, V. A., Efthymoglou, G. P., & Chayawan, C. 2007, IEEE Communications letlers, 11, 985
Abramowitz, M. & Stegun, I. 1964, Handbook of Mathematical Functions
Benoît, A., Ade, P., Amblard, A., et al. 2004, A&A, 424, 571
Bernard, J.-P., Ade, P., De Bernardis, P., et al. 2007, in EAS Publications Series, Vol. 23, EAS Publications Series, ed. M.-A. Miville-Deschênes & F. Boulanger, 189–203
Boissier, J., Bockelée-Morvan, D., Biver, N., et al. 2009, Earth Moon and Planets, 105, 89
Clarke, D., Naghizadeh-Khouei, J., Simmons, J. F. L., & Stewart, B. G. 1993, A&A, 269, 617
Dotson, J. L., Vaillancourt, J. E., Kirby, L., et al. 2010, ApJS, 186, 406
Dowell, C. D., Hildebrand, R. H., Schleuning, D. A., et al. 1998, ApJ, 504, 588
Fissel, L. M., Ade, P. A. R., Angilè, F. E., et al. 2010, in Society of Photo-Optical Instrumentation Engineers (SPIE) Conference Series, Vol. 7741, Society of Photo-Optical Instrumentation Engineers (SPIE) Conference Series
Girart, J. M., Rao, R., & Marrone, D. P. 2006, Science, 313, 812
Gradshteyn, I. S. & Ryzhik, I. M. 2007, Table of Integrals, Series, and Products
Greaves, J. S., Holland, W. S., Jenness, T., et al. 2003, MNRAS, 340, 353
Li, H., Dowell, C. D., Kirby, L., Novak, G., & Vaillancourt, J. E. 2008, Appl. Opt., 47, 422
Mood, A. M. & Graybill, A. F. 1974, Introduction to the Sheory of Statistics, 3rd ed. McGraw-Hill, New-York
Naghizadeh-Khouei, J. & Clarke, D. 1993, A&A, 274, 968
Page, L., Hinshaw, G., Komatsu, E., et al. 2007, ApJS, 170, 335
Pérez-Sánchez, A. F. & Vlemmings, W. H. T. 2013, A&A, 551, A15
Platt, S. R., Hildebrand, R. H., Pernic, R. J., Davidson, J. A., & Novak, G. 1991, PASP, 103, 1193
Quinn, J. L. 2012, A&A, 538, A65
Renbarger, T., Chuss, D. T., Dotson, J. L., et al. 2004, PASP, 116, 415
Rice, S. O. 1945, Bell Systems Tech. J., Volume 24, p. 46-156, 24, 46
Schleuning, D. A., Dowell, C. D., Hildebrand, R. H., Platt, S. R., & Novak, G. 1997, PASP, 109, 307
Serkowski, K. 1958, Acta Astron., 8, 135
Serkowski, K. 1962, Advances in Astronomy and Astrophysics, 0, 290
Simmons, J. F. L. & Stewart, B. G. 1985, A&A, 142, 100
Tauber, J. A., Mandolesi, N., Puget, J., et al. 2010, A&A, 520, A1
Thum, C., Wiesemeyer, H., Paubert, G., Navarro, S., & Morris, D. 2008, PASP, 120, 777
Vaillancourt, J. E. 2006, PASP, 118, 1340
Vaillancourt, J. E. & Matthews, B. C. 2012, ApJS, 201, 13
Vinokur, M. 1965, Annales d'Astrophysique, 28, 412
Wardle, J. F. C. & Kronberg, P. P. 1974, ApJ, 194, 249

Appendix A: Expressions for PDFs

Here we present expressions for the 2D probability density functions, which are discussed in Section 2:

$$f(I,p,\psi\,|\,I_0,p_0,\psi_0,\Sigma) = \frac{2|p|\,I^2}{\sqrt{(2\pi)^3\sigma^3}}\,\exp\left(-\frac{1}{2}\begin{bmatrix} I-I_0 \\ p\,I\,\cos(2\psi)-p_0\,I_0\cos(2\psi_0) \\ p\,I\,\sin(2\psi)-p_0\,I_0\sin(2\psi_0)\end{bmatrix}^{\mathrm{T}}\Sigma^{-1}\begin{bmatrix} I-I_0 \\ p\,I\,\cos(2\psi)-p_0\,I_0\,\cos(2\psi_0) \\ p\,I\,\sin(2\psi)-p_0\,I_0\,\sin(2\psi_0)\end{bmatrix}\right); \tag{A.1}$$

$$f_{2\mathrm{D}}(p,\psi\,|\,I_0,p_0,\psi_0,\Sigma) = \frac{|p|}{2\pi\sigma^3}\exp\left(-\frac{I_0^2}{2}\gamma\right)\left\{\sqrt{\frac{2}{\pi}}\frac{\beta I_0}{\alpha^2}+\frac{1}{\alpha^{3/2}}\left[1+\frac{\beta^2 I_0^2}{\alpha}\right]\exp\left(\frac{\beta^2 I_0^2}{2\alpha}\right)\left[1+\mathrm{erf}\left(\frac{\beta I_0}{\sqrt{2\alpha}}\right)\right]\right\} \quad \text{for} \quad p\geqslant 0; \tag{A.2}$$

$$f_{2\mathrm{D}}(p,\psi\,|\,I_0,p_0,\psi_0,\Sigma) = \frac{|p|}{2\pi\sigma^3}\exp\left(-\frac{I_0^2}{2}\gamma\right)\left\{-\sqrt{\frac{2}{\pi}}\frac{\beta I_0}{\alpha^2}+\frac{1}{\alpha^{3/2}}\left[1+\frac{\beta^2 I_0^2}{\alpha}\right]\exp\left(\frac{\beta^2 I_0^2}{2\alpha}\right)\left[1-\mathrm{erf}\left(\frac{\beta I_0}{\sqrt{2\alpha}}\right)\right]\right\} \quad \text{for} \quad p\leqslant 0; \tag{A.3}$$

$$f_{2\mathrm{D}}(p,\psi\,|\,p_0,\psi_0,\Sigma_{\mathrm{p}}) = \frac{p}{\pi\sigma_{\mathrm{p,G}}^2}\,\exp\left(-\frac{1}{2}\begin{bmatrix} p\,\cos(2\psi)-p_0\cos(2\psi_0) \\ p\,\sin(2\psi)-p_0\sin(2\psi_0)\end{bmatrix}^{\mathrm{T}}\Sigma_{\mathrm{p}}^{-1}\begin{bmatrix} p\,\cos(2\psi)-p_0\,\cos(2\psi_0) \\ p\,\sin(2\psi)-p_0\,\sin(2\psi_0)\end{bmatrix}\right) \quad \text{for} \quad \sigma_{\mathrm{I}}=0. \tag{A.4}$$

Appendix B: Computation of $f_{2\mathrm{D}}$

The 3D PDF of (I,p,ψ) is given by

$$f(I,p,\psi) = 2\,|p|\,I^2\,F\,(I,pI\cos 2\psi,pI\sin 2\psi)\,. \tag{B.1}$$

To compute the 2D PDF of (p,ψ) we marginalize over total intensity. However, some care is required here, because the above expression for $f(I,p,\psi)$ is only valid for $pI\geqslant 0$ (i.e., we cannot measure negative p unless I happens to be negative due to noise) and f must be taken to be null otherwise. This means that the marginalization is performed over $I\geqslant 0$ for positive p and over $I\leqslant 0$ for negative p:

$$f_{2\mathrm{D}} = \int_0^{+\infty} 2\,|p|\,I^2\,F\,(I,pI\cos 2\psi,pI\sin 2\psi)\,dI, \quad \text{for} \quad p\geqslant 0; \tag{B.2}$$

$$f_{2\mathrm{D}} = \int_{-\infty}^{0} 2\,|p|\,I^2\,F\,(I,pI\cos 2\psi,pI\sin 2\psi)\,dI, \quad \text{for} \quad p\leqslant 0. \tag{B.3}$$

The integrand may be written so as to exhibit the dependence on total intensity,

$$f = \frac{2\,|p|\,I^2}{(2\pi)^{3/2}\sigma^3}\exp\left[-\frac{1}{2}\left(I^2\alpha-2I I_0\beta+I_0^2\gamma\right)\right] \tag{B.4}$$

and then we make use of the functions (Gradshteyn & Ryzhik 2007):

$$G_-(x,y) = \int_{-\infty}^{0} I^2 e^{-xI^2+2yI}dI \;\; = -\frac{y}{2x^2}+\sqrt{\frac{\pi}{x^5}}\frac{2y^2+x}{4}\exp\left(\frac{y^2}{x}\right)\left[1-\mathrm{erf}\left(\frac{y}{\sqrt{x}}\right)\right]; \tag{B.5}$$

$$G_+(x,y) = \int_{0}^{+\infty} I^2 e^{-xI^2+2yI}dI = \frac{y}{2x^2}+\sqrt{\frac{\pi}{x^5}}\;\frac{2y^2+x}{4}\exp\left(\frac{y^2}{x}\right)\left[1+\mathrm{erf}\left(\frac{y}{\sqrt{x}}\right)\right]. \tag{B.6}$$

Elementary replacement of (x,y) by $(\alpha/2, I_0\beta/2)$ yields the PDF of Eqs. A.2 and A.3, given in the main body of the text.

Appendix C: Illustrations of $f_{2\mathrm{D}}$

We illustrate the shape of the 2D probability density function $f_{2\mathrm{D}}(p,\psi\,|\,I_0,p_0,\psi_0,\Sigma)$ in Fig. F.1, for the case of a perfectly known intensity having no correlation with the polarization. Starting from a given couple of true polarization parameters $\psi_0=0°$ and $p_0=0.1$, the PDF is computed for various signal-to-noise ratios $p_0/\sigma_{\mathrm{p,G}}$ and settings of the covariance matrix. The signal-to-noise ratio $p_0/\sigma_{\mathrm{p,G}}$ is varied from 0.01 to 0.5, 1, and 5 (top to bottom). The dashed crossing lines show the location of the initial true polarization values. The leftmost column shows the results obtained when the covariance matrix is assumed to be diagonal and symmetric, (i.e., $\varepsilon=1$ and $\rho=0$), as was usually done in previous works on polarization data. The distribution along the ψ axis is fully symmetric around 0, implying the absence of bias on the polarization angle. When varying the ellipticity ε from 1/2 to 2 (columns 2 and 3), we still observe symmetrical PDFs in this configuration, but multiple peaks appear at low signal-to-noise ratio. In the presence of correlation, i.e., $\rho=-1/2$ and $1/2$ (columns 4 and 5), the maximum peak is now slightly shifted in p and ψ, with an asymmetric PDF around the initial ψ_0 value.

In the usual canonical case, $\varepsilon = 1$ and $\rho = 0$, the PDF remains strictly symmetric whatever the value of the initial true polarization angle ψ_0. However, when changing the true polarization angle ψ_0, as shown in Fig. F.2, the PDF may become asymmetrical once the ellipticity $\varepsilon \neq 1$ or the correlation $\rho \neq 0$. This will induce a statistical bias in the measurement of the polarization angle ψ, which could be positive or negative depending on the covariance matrix and the true value ψ_0, as discussed in Sect. 3.

Examples of 2D probability density functions, $f_{2D}(p, \psi \,|\, I_0, p_0, \psi_0, \mathbf{\Sigma})$, for finite values of I_0/σ_I (1, 2, and 5), and various ε and ρ situations, are shown in Fig. F.3, for the case $\rho_Q = \rho_U = 0$. The true polarization parameters are $p_0 = 0.1$ and $\psi_0 = 0°$, and the polarization signal-to-noise ratio is set to $p_0/\sigma_{p,G} = 1$, so these plots may be directly compared to the third row of Fig. F.1. The effect of varying I_0/σ_I on the global shape of the PDF seems rather small, but the position of the maximum likelihood in (p, ψ) is noticeably changed to lower values of p when $I_0/\sigma_I \lesssim 2$, while the mean likelihood appears to be increased.

Appendix D: General PDF of p and ψ

In the context of communication network science Aalo et al. (2007) derived full expressions for the probability density functions of envelope and phase quantities in the general case. These expressions can be directly translated to express the PDF of the polarization fraction and angle, p and ψ.

We can apply the rotation of the covariance introduced in Sect. 2.1 by an angle θ, given by Eq. 5, to remove the correlation term between the Stokes parameters. We define the mean and the variance of the normalized Stokes parameters in this new frame by

$$\mu_1 = p_0 \cos(2\psi_0 - \theta), \quad \mu_2 = p_0 \sin(2\psi_0 - \theta) \tag{D.1}$$

and

$$\sigma_1^2 = (\sigma_Q^2 \cos^2\theta + \sigma_U^2 \sin^2\theta + \rho\sigma_Q\sigma_U \sin 2\theta) / I_0^2, \quad \sigma_2^2 = (\sigma_Q^2 \sin^2\theta + \sigma_U^2 \cos^2\theta - \rho\sigma_Q\sigma_U \sin 2\theta) / I_0^2. \tag{D.2}$$

The probability density function of p is now written as

$$f_p(p \,|\, p_0, \psi_0, \mathbf{\Sigma}_p) = \frac{p}{2\sigma_1\sigma_2} \exp\left\{-\frac{1}{2}\left[\frac{\mu_1^2}{\sigma_1^2} + \frac{\mu_2^2}{\sigma_2^2} + \frac{p^2}{2}\left(\frac{1}{\sigma_1^2} + \frac{1}{\sigma_2^2}\right)\right]\right\} \times \sum_{n=0}^{\infty} \frac{\zeta_n \mathcal{I}_n\left(\frac{p^2}{4}\left(\frac{1}{\sigma_2^2} - \frac{1}{\sigma_1^2}\right)\right)}{\left[\left(\frac{\mu_1}{\sigma_1^2}\right)^2 + \left(\frac{\mu_2}{\sigma_2^2}\right)^2\right]^n} \left\{ \mathcal{I}_{2n}\left(p\sqrt{\left(\frac{\mu_1}{\sigma_1^2}\right)^2 + \left(\frac{\mu_2}{\sigma_2^2}\right)^2}\right) \sum_{k=0}^{n} \delta_k C_k^n \left[\left(\frac{\mu_1}{\sigma_1^2}\right)^2 - \left(\frac{\mu_2}{\sigma_2^2}\right)^2\right]^{n-k} \left(2\frac{\mu_1\mu_2}{\sigma_1^2\sigma_2^2}\right)^k \right\}, \tag{D.3}$$

with $\mathcal{I}_n$ the nth order modified Bessel function of the first kind. Here $\zeta_0 = 1$ and $\zeta_n = 2$ for $n \neq 0$, $C_k^n \equiv n!/k!(n-k)!$ are binomial coefficients, and δ_k is defined by

$$\delta_k = \begin{cases} 0 & \text{for } k \text{ odd}, \\ 2\,(-1)^{k/2} & \text{for } k \text{ even}. \end{cases} \tag{D.4}$$

It should be noted that the above expression converges so fast that only a few terms of the infinite sum are required to obtain sufficient accuracy. On the other hand, the probability density function of the polarization angle is given by

$$f_\psi(\psi \,|\, p_0, \psi_0, \mathbf{\Sigma}_p) = \exp\left[-\frac{1}{1-\rho^2}\left(\frac{Q_0^2}{2\sigma_Q^2} + \frac{U_0^2}{2\sigma_U^2} - \frac{\rho Q_0 U_0}{\sigma_Q\sigma_U}\right)\right] \times \frac{\sqrt{1-\rho^2}}{\pi\sigma_Q\sigma_U\mathcal{A}(\psi)} \left\{1 + \frac{\sqrt{\pi}\mathcal{B}(\psi)}{\sqrt{\mathcal{A}(\psi)}} \exp\left[\frac{\mathcal{B}^2(\psi)}{\mathcal{A}(\psi)}\right] \mathrm{erfc}\left[-\frac{\mathcal{B}(\psi)}{\sqrt{\mathcal{A}(\psi)}}\right]\right\}, \tag{D.5}$$

where

$$\mathcal{A}(\psi) = \frac{2\cos^2 2\psi}{\sigma_Q^2} + \frac{2\sin^2 2\psi}{\sigma_U^2} - 4\frac{\rho \sin 2\psi \cos 2\psi}{\sigma_Q\sigma_U}, \tag{D.6}$$

$$\mathcal{B}(\psi) = \frac{1}{\sqrt{1-\rho^2}}\left[\frac{\cos 2\psi}{\sigma_Q}\left(\frac{Q_0}{\sigma_Q} - \frac{\rho U_0}{\sigma_U}\right) + \frac{\sin 2\psi}{\sigma_U}\left(\frac{U_0}{\sigma_U} - \frac{\rho Q_0}{\sigma_Q}\right)\right], \tag{D.7}$$

and

$$\mathrm{erfc}(z) = \frac{2}{\sqrt{\pi}} \int_z^\infty \exp[-x^2] dx \tag{D.8}$$

is the complementary error function.

Appendix E: Impact of ρ_Q and ρ_U on ε and ρ

The covariance matrix Σ is positive definite, so may be written as a Cholesky product $\Sigma = \mathsf{L}^T\mathsf{L}$, with

$$\mathsf{L} = \begin{pmatrix} L_{11} & 0 & 0 \\ L_{12} & L_{22} & 0 \\ L_{13} & L_{23} & L_{33} \end{pmatrix}. \tag{E.1}$$

The six L_{ij} are independent, unlike the six parameters of the covariance matrix, $(\sigma_I, \sigma_Q, \sigma_U, \rho, \rho_Q, \rho_U)$, or the parameters that we use in this paper, $(\sigma_I, \sigma_Q, \varepsilon, \rho, \rho_Q, \rho_U)$. In the general case, these are given in terms of the L_{ij} as (assuming I_0=1)

$$\rho = \frac{L_{12}L_{13} + L_{22}L_{23}}{\sqrt{\left(L_{12}^2 + L_{22}^2\right)\left(L_{13}^2 + L_{23}^2 + L_{33}^2\right)}}, \quad \varepsilon = \sqrt{\frac{L_{13}^2 + L_{23}^2 + L_{33}^2}{L_{12}^2 + L_{22}^2}},$$
$$\rho_Q = \frac{L_{12}}{\sqrt{L_{12}^2 + L_{22}^2}}, \quad \text{and} \quad \rho_U = \frac{L_{13}}{\sqrt{L_{13}^2 + L_{23}^2 + L_{33}^2}}. \tag{E.2}$$

When there is no correlation between I and the Q or U components, then $L_{12} = L_{13}$=0, which leads to the following system:

$$\rho = \rho_0 = \frac{L_{22}L_{23}}{|L_{22}|\sqrt{L_{23}^2 + L_{33}^2}}; \quad \varepsilon = \varepsilon_0 = \frac{\sqrt{L_{23}^2 + L_{33}^2}}{|L_{22}|}. \tag{E.3}$$

The ellipticity and the correlation coefficient are therefore modified by the presence of the correlation between I and (Q, U). A little algebra leads to expressions for ε and ρ as functions of ε_0, ρ_0, ρ_Q, and ρ_U, namely

$$\varepsilon = \varepsilon_0\sqrt{\frac{1-\rho_Q^2}{1-\rho_U^2}} \qquad \text{and} \qquad \rho = \rho_Q\rho_U + \rho_0\sqrt{\left(1-\rho_Q^2\right)\left(1-\rho_U^2\right)}, \tag{E.4}$$

which are Eqs. 27.

Appendix F: Derivation of classical uncertainties

We describe here how the expressions for the classical uncertainties of p and ψ, introduced in Sect. 4.3, are obtained from the derivatives of p and ψ. We first note that we generally have

$$\sigma_X^2 = E\left[(X - E[X])^2\right] = E\left[(dX)^2\right], \tag{F.1}$$

where $dX = X - E[X]$ is an infinitesimal element.

The classical uncertainty of p can therefore be given by the expression $\sigma_{p,C}^2 = E\left[(dp)^2\right]$. Using the expression for p we obtain

$$\begin{aligned}(dp)^2 &= \left(\frac{\partial p}{\partial Q}dQ + \frac{\partial p}{\partial U}dU + \frac{\partial p}{\partial I}dI\right)^2 \\ &= \left(\frac{\partial p}{\partial Q}\right)^2(dQ)^2 + \left(\frac{\partial p}{\partial U}\right)^2(dU)^2 + \left(\frac{\partial p}{\partial I}\right)^2(dI)^2 + 2\frac{\partial p}{\partial Q}\frac{\partial p}{\partial U}dQdU + 2\frac{\partial p}{\partial Q}\frac{\partial p}{\partial I}dQdI + 2\frac{\partial p}{\partial U}\frac{\partial p}{\partial I}dUdI,\end{aligned} \tag{F.2}$$

where the partial derivatives are

$$\frac{\partial p}{\partial Q} = \frac{1}{2}\frac{2Q}{I\sqrt{Q^2+U^2}} = \frac{Q}{pI^2}, \qquad \frac{\partial p}{\partial U} = \frac{1}{2}\frac{2U}{I\sqrt{Q^2+U^2}} = \frac{U}{pI^2}, \qquad \text{and} \qquad \frac{\partial p}{\partial I} = -\frac{\sqrt{Q^2+U^2}}{I^2} = -\frac{p}{I}. \tag{F.3}$$

This leads to the following expression for the classical uncertainty:

$$\begin{aligned}\sigma_{p,C}^2 &= \frac{1}{p^2I^4}E\left[Q^2(dQ)^2 + U^2(dU)^2 + p^4I^2(dI)^2 + 2QUdQdU - 2QIp^2dQdI - 2UIp^2dUdI\right] \\ &= \frac{1}{p^2I^4}\Big(Q^2E\left[(Q-E[Q])^2\right] + U^2E\left[(U-E[U])^2\right] + p^4I^2E\left[(I-E[I])^2\right] \\ &\quad + 2QUE\left[(Q-E[Q])(U-E[U])\right] - 2QIp^2E\left[(Q-E[Q])(I-E[I])\right] - 2UIp^2E\left[(U-E[U])(I-E[I])\right]\Big).\end{aligned} \tag{F.4}$$

This finally leads to

$$\sigma_{p,C}^2 = \frac{1}{p^2I^4}\left(Q^2\sigma_Q^2 + U^2\sigma_U^2 + p^4I^2\sigma_I^2 + 2QU\sigma_{QU} - 2IQp^2\sigma_{IQ} - 2IUp^2\sigma_{IU}\right). \tag{F.5}$$

Similarly we can derive an expression for the non-classical uncertainty of the polarization angle, ψ, given by $\sigma^2_{\psi,\mathrm{C}} = E\left[(d\psi)^2\right]$. Using the expression of ψ, we obtain the partial derivatives

$$\frac{\partial\psi}{\partial U} = \frac{1}{2}\frac{Q}{Q^2+U^2} \qquad \text{and} \qquad \frac{\partial\psi}{\partial Q} = -\frac{1}{2}\frac{U}{Q^2+U^2}, \tag{F.6}$$

as well as an expression for the classical ψ uncertainty:

$$\begin{aligned}\sigma^2_{\psi,\mathrm{C}} = E\left[\left(\frac{\partial\psi}{\partial U}dU + \frac{\partial\psi}{\partial Q}dQ\right)^2\right] = E\left[\left(\frac{QdU - UdQ}{2p^2I^2}\right)^2\right] = E\left[\frac{Q^2dU^2 + U^2dQ^2 - 2QUdQdU}{4p^4I^4}\right] \\ = \frac{Q^2\sigma_{\mathrm{UU}} + U^2\sigma_{\mathrm{QQ}} - 2QU\sigma_{\mathrm{QU}}}{4p^4I^4}.\end{aligned} \tag{F.7}$$

Using Eq. F.5 and assuming $\sigma_{\mathrm{II}} = \sigma_{\mathrm{IQ}} = \sigma_{\mathrm{IU}} = 0$, we find

$$p^2I^4 = \frac{Q^2\sigma^2_{\mathrm{Q}} + U^2\sigma^2_{\mathrm{U}} + 2QU\sigma_{\mathrm{QU}}}{\sigma^2_{\mathrm{p,C}}}, \tag{F.8}$$

and replacing this expression in Eq. F.7 finally leads to

$$\sigma_{\psi,\mathrm{C}} = \sqrt{\frac{Q^2\sigma^2_{\mathrm{U}} + U^2\sigma^2_{\mathrm{Q}} - 2QU\sigma_{\mathrm{QU}}}{Q^2\sigma^2_{\mathrm{Q}} + U^2\sigma^2_{\mathrm{U}} + 2QU\sigma_{\mathrm{QU}}}} \times \frac{\sigma_{\mathrm{p,C}}}{2p}. \tag{F.9}$$

Notice that the above two expressions for the classical estimates have been obtained in the small-error limit, and therefore they are formally inapplicable to the large uncertainty regime. In Sect. 4 we discuss the extent to which they can provide reasonable proxies for the errors, even at low S/N.

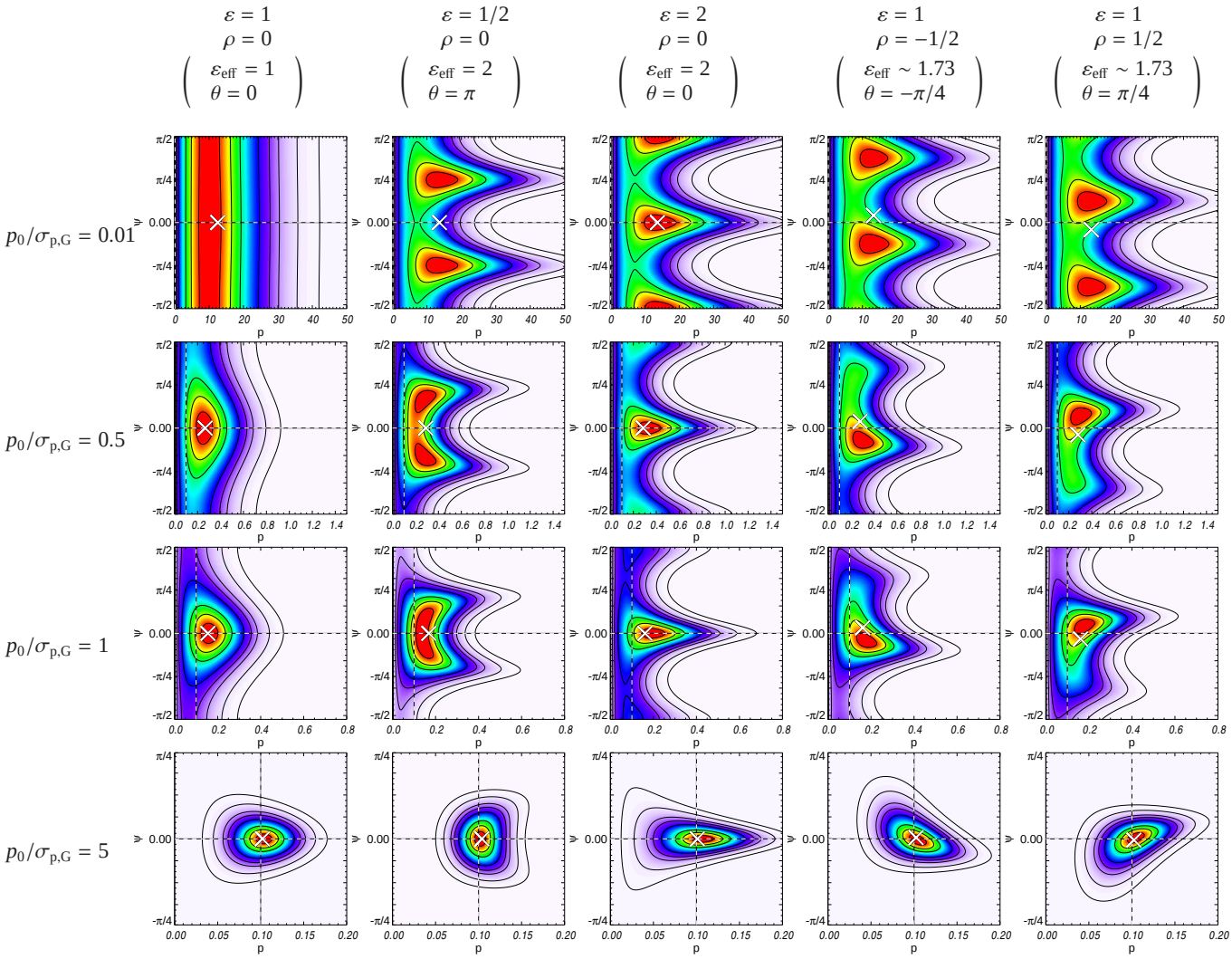

Fig. F.1. Probability density functions, $f_{2D}(p, \psi \mid p_0, \psi_0, \Sigma_p)$, with infinite S/N on intensity, computed for a given set of polarization parameters, namely $\psi_0 = 0°$ and $p_0 = 0.1$ (dashed lines). Each row corresponds to a specific level of the signal-to-noise ratio $p_0/\sigma_{p,G} = 0.01, 0.5, 1$, and 5, from top to bottom. Various configurations of the covariance matrix are shown (in the different columns). Furthest left is the standard case: no ellipticity and no correlation. The next two columns show the impact of ellipticities $\varepsilon = 1/2$ and 2. The last two columns deal with correlations $\rho = -1/2$ and $+1/2$. White crosses indicate the mean likelihood estimates of the PDF $(\overline{p}, \overline{\psi})$. The contour levels are shown at 0.1, 1, 5, 10, 20, 50, 70, and 90% of the maximum of the distribution.

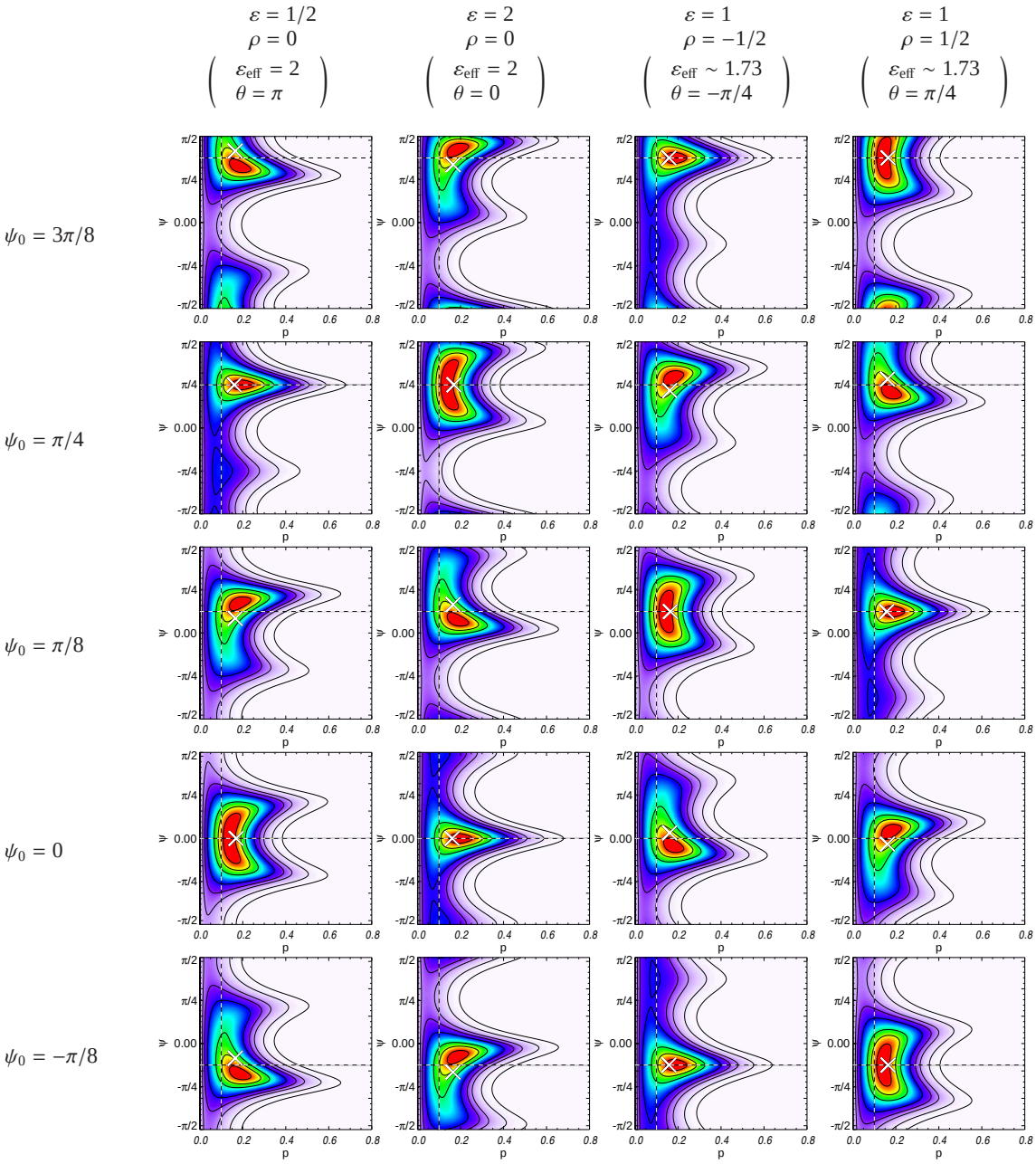

Fig. F.2. Probability density functions, $f_{\rm 2D}(p, \psi \,|\, p_0, \psi_0, \mathbf{\Sigma}_{\rm p})$, plotted for various values of ψ_0 (rows), spanning from $-\pi/8$ to $3\pi/8$, and computed for four configurations of the covariance matrix (columns), parameterized by ε and ρ. The signal-to-noise on the intensity I is assumed to be infinite here. A true value of polarization $p_0 = 0.1$ has been chosen, and with S/N $p_0/\sigma_{\rm p,G}$=1. White crosses indicate the mean likelihood estimates of the PDF $(\overline{p}, \overline{\psi})$. The contour levels are provided at 0.1, 1, 5, 10, 20, 50, 70, and 90% of the maximum of the distribution.

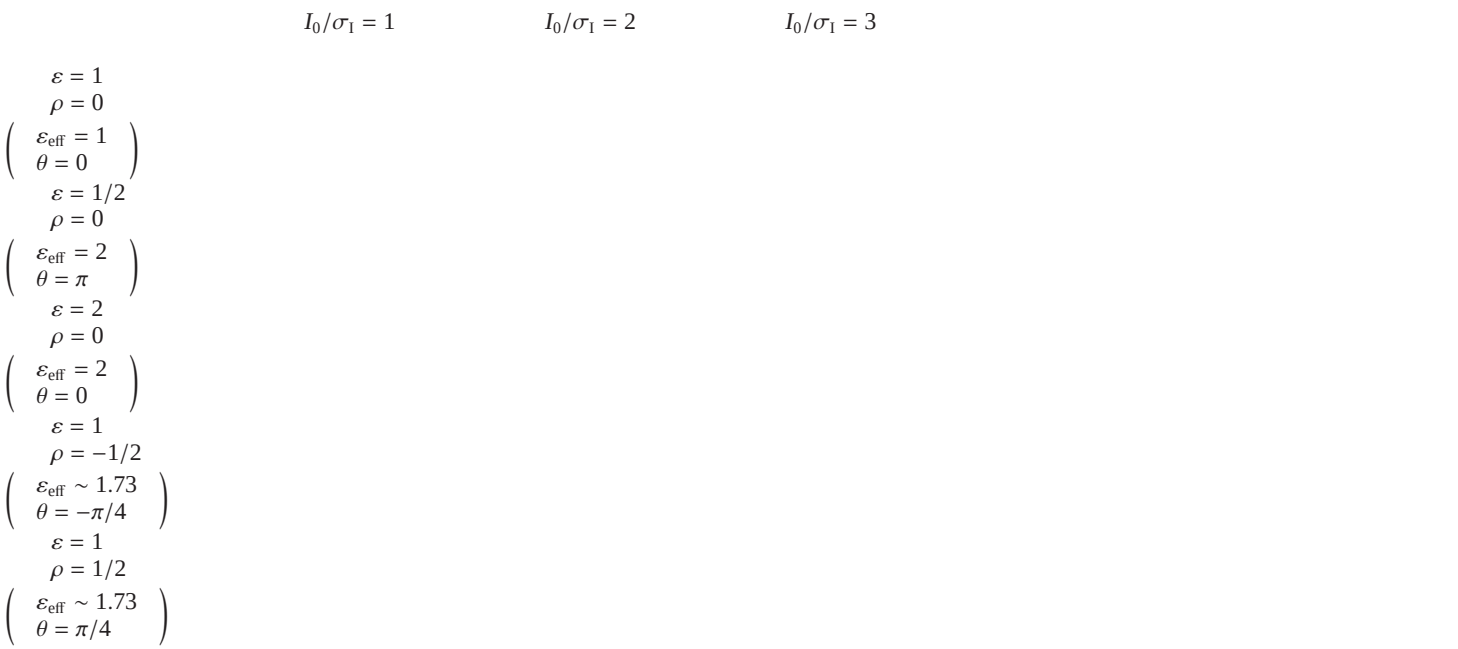

Fig. F.3. Probability density functions, $f_{2D}(p, \psi \,|\, I_0,\ p_0, \psi_0, \Sigma)$, with finite S/N on intensity, $I_0/\sigma_I = 1$, 2, and 5 (columns from left to right), computed for a given set of polarization parameters, $\psi_0 = 0°$ and $p_0 = 0.1$ (dashed lines), and a signal-to-noise ratio on the polarized intensity set to $p_0/\sigma_{p,G} = 1$. Correlation coefficients ρ_Q and ρ_U are set to zero. Various configurations of the covariance matrix are shown (rows). White crosses indicate the mean likelihood estimates of the PDF $(\overline{p}, \overline{\psi})$. The contour levels are provided at 0.1, 1, 5, 10, 20, 50, 70, and 90% of the maximum of the distribution. Note that the polarization fraction is here defined over both the negative and positive ranges, due to the noise of the intensity.